Article

Cell Reports

Adult sox10^{+} Cardiomyocytes Contribute to Myocardial Regeneration in the Zebrafish

Graphical Abstract

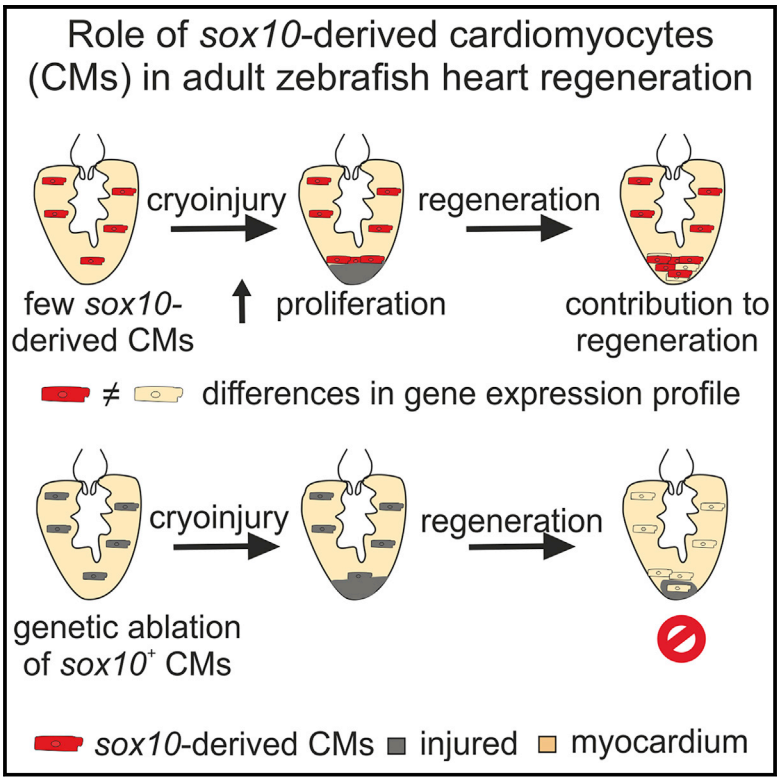

Highlights

- Adult *sox10*-derived cardiomyocytes contribute to zebrafish heart regeneration
- *sox10*-derived cardiomyocytes have a high proliferation index
- *sox10*-derived cardiomyocytes have a distinct gene expression profile
- Genetic ablation of sox10-derived cells impairs heart regeneration

Authors

Marcos Sande-Melón, Inês J. Marques, María Galardi-Castilla, ..., Vladimir Benes, Rémy Bruggmann, Nadia Mercader

Correspondence

nadia.mercader@ana.unibe.ch

In Brief

Unlike adult mammals, zebrafish regenerate their heart after injury through proliferation of preexistent cardiomyocytes. Sande-Melón et al. identify a subset of *sox10*-positive cardiomyocytes within the uninjured heart with a high capacity to contribute to the new myocardium. Ablation of these cardiomyocytes confirms that they play an essential role during heart regeneration.

Sande-Melón et al., 2019, Cell Reports *29*, 1041–1054
October 22, 2019
https://doi.org/10.1016/j.celrep.2019.09.041

CellPress

Cell Reports
Article

Adult sox10^{+} Cardiomyocytes Contribute to Myocardial Regeneration in the Zebrafish

Marcos Sande-Melón,[1,2] Inês J. Marques,[2] María Galardi-Castilla,[1] Xavier Langa,[2] María Pérez-López,[1,6] Marius-Alexandru Botos,[2] Héctor Sánchez-Iranzo,[1,7] Gabriela Guzmán-Martínez,[1,3] David Miguel Ferreira Francisco,[4] Dinko Pavlinic,[5,8] Vladimir Benes,[5] Rémy Bruggmann,[4] and Nadia Mercader[1,2,9,*]

[1]Spanish National Centre for Cardiovascular Research Carlos III (CNIC-ISCIII), 28029 Madrid, Spain
[2]Institute of Anatomy, University of Bern, 3012 Bern, Switzerland
[3]Departamento de Cardiología, Hospital Universitario La Paz. IdiPaz, 28046 Madrid, Spain
[4]Interfaculty Bioinformatics Unit and Swiss Institute of Bioinformatics, University of Bern, 3012 Bern, Switzerland
[5]Genomics Core Facility, European Molecular Biology Laboratory (EMBL) Heidelberg, 69117 Heidelberg, Germany
[6]Present address: Instituto de Investigaciones Biomédicas Alberto Sols, 28029 Madrid, Spain
[7]Present address: European Molecular Biology Laboratory EMBL, 69117 Heidelberg, Germany
[8]Present address: Single Cell Genomics Platform, Institute of Molecular and Clinical Ophthalmology Basel, 4031 Basel, Switzerland
[9]Lead Contact
*Correspondence: nadia.mercader@ana.unibe.ch
https://doi.org/10.1016/j.celrep.2019.09.041

SUMMARY

During heart regeneration in the zebrafish, fibrotic tissue is replaced by newly formed cardiomyocytes derived from preexisting ones. It is unclear whether the heart is composed of several cardiomyocyte populations bearing different capacity to replace lost myocardium. Here, using *sox10* genetic fate mapping, we identify a subset of preexistent cardiomyocytes in the adult zebrafish heart with a distinct gene expression profile that expanded after cryoinjury. Genetic ablation of *sox10*$^{+}$ cardiomyocytes impairs cardiac regeneration, revealing that these cells play a role in heart regeneration.

INTRODUCTION

Cardiomyocyte (CM) renewal in the human heart is marginal and, after acute myocardial infarction, millions of CMs are irreversibly lost and replaced by a fibrotic scar (Prabhu and Frangogiannis, 2016). Adult mammalian CMs have a poor capacity to proliferate, and an efficient contribution of an adult stem cell pool for myocardial replacement has not been demonstrated (Lerman et al., 2016). By contrast, zebrafish have an extraordinary capacity for heart regeneration after injury (González-Rosa et al., 2017; Kikuchi, 2014). Lineage tracing studies have revealed that preexisting CMs are the origin of *de novo* formed cardiac muscle (Jopling et al., 2010; Kikuchi et al., 2010). Upon injury, CMs adjacent to the injury lose their sarcomeric organization and exhibit a more immature phenotype. Concomitant with this structural change, CMs were described to express developmental genes, suggesting a reversion of their differentiated phenotype to a more embryonic-like state (Lepilina et al., 2006). Indeed, *gata4*, *hand2*, and *tbx5a*, which play key roles during heart development (Garrity et al., 2002; Grajevskaja et al., 2018; Kuo et al., 1997; Molkentin et al., 1997; Srivastava et al., 1997), are required for heart regeneration (Grajevskaja et al., 2018; Gupta et al., 2013; Schindler et al., 2014). Moreover, CMs contributing to heart regeneration activate *gata4* and *ctgfa* enhancer elements upon injury (Gupta et al., 2013; Kikuchi et al., 2010; Pfefferli and Jaźwińska, 2017). While CMs that will contribute to heart regeneration upregulate a specific set of genes, it is unclear whether CM subsets contributing to regeneration can be distinguished by means of their expression profile in the uninjured heart.

Like mammals, zebrafish CMs derive from first and second heart field progenitors (de Pater et al., 2009; Mosimann et al., 2015; Zhou et al., 2011). However, in the zebrafish, the neural crest represents a third progenitor population that contributes to the developing heart. Cell transplantation and fluorescent dye tracing experiments suggested that cardiac neural crest cells incorporate not only into the areas of the outflow tract, as in mammals and birds, but also into the atrium and ventricle (Li et al., 2003; Sato and Yost, 2003). Moreover, genetic lineage tracing using *sox10* as a neural crest cell marker revealed a cellular contribution of *sox10*$^{+}$ cells to the zebrafish heart (Cavanaugh et al., 2015; Mongera et al., 2013) and suggested that *sox10*-derived CMs are necessary for correct heart development (Abdul-Wajid et al., 2018). Noteworthy, it is still unclear if a *sox10*$^{+}$ neural crest population differentiates into CMs or if alternatively, a *sox10*$^{+}$ CM subset is relevant for heart development.

Here, we assessed the contribution of *sox10*-derived cells to the adult zebrafish heart using *sox10*:CreER^{T2} fate mapping during homeostasis and regeneration. We found that embryonic *sox10*-derived cells contributed to significant portions of the adult heart. We also identified adult *sox10*$^{+}$ CMs that expanded to a higher degree upon injury than other CMs and significantly contributed to cardiac regeneration. Their transcriptome differed from other CMs in the heart, and their genetic ablation impaired recovery from ventricular cryoinjury.

RESULTS

sox10-Expressing Cells Contribute to the Regenerated Myocardium

sox10-derived cells were proposed to contribute to the adult zebrafish heart (Abdul-Wajid et al., 2018). Since a non-inducible

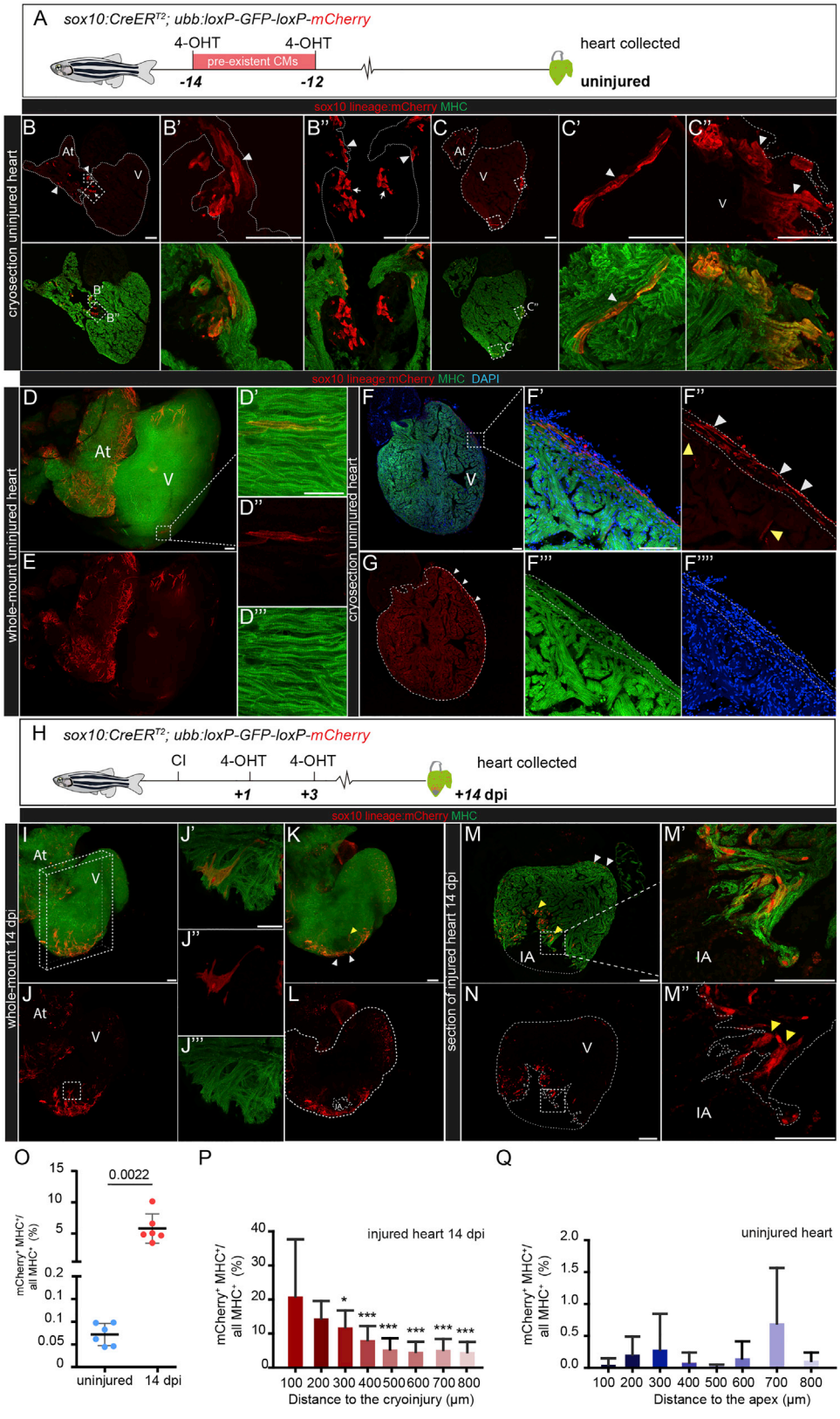

(legend on next page)

sox10:Cre line was used for these studies, it was not clear whether embryonic *sox10*$^+$ cells or adult *sox10*$^+$ contributed to the adult zebrafish heart. To clarify the source of *sox10*-derived cells contributing to the adult heart, we used the line *Tg(sox10:CreER^{T2})* (Mongera et al., 2013), in which CreER is driven by the −4.9-kb *sox10* promoter (Carney et al., 2006). This line was crossed with *Tg(ubb:loxP-GFP-loxP-mCherry)* (Mosimann et al., 2011), from now on named *ubb:Switch* (Figure 1A). In double-transgenic animals, 4-hydroxytamoxifen (4-OHT) administration leads to constitutive mCherry expression in cells expressing *sox10:CreER^{T2}* at the time of recombination (Figure 1A). Recombination in adult *sox10:CreER^{T2};ubb:Switch* zebrafish led to the activation of mCherry expression in a few cardiac cells in the atrium, ventricle, and valves (Figures 1B–1G). We observed both *sox10*-derived CMs (mCherry$^+$/MHC$^+$) (Figures 1B′–1C‴, 1D′ –1D‴, and 1F′ –1F⁗) and non-CMs (only mCherry$^+$) (Figure 1B″), the latter mostly contributing to the valves. Thus, the adult heart bears a very small population of CMs present with an active *sox10*-promoter element.

We next wanted to assess if *sox10*-derived cells contribute to heart regeneration. When 4-OHT treatment was performed shortly after ventricular cryoinjury (Figure 1H), we observed an expansion of *sox10*-derived cells (Figures 1I–1O). Immunostainings confirmed that *sox10*-derived cells were CMs, as they co-expressed the myocardial marker myosin heavy chain (MHC) (Figures 1J′–J‴ and 1M′–M″). In order to estimate the contribution of *sox10*-derived CMs during the regeneration process, we measured the ratio of *sox10*-derived CMs (mCherry$^+$/ MHC$^+$) versus other CMs (MHC$^+$) in the entire heart (Figure 1O). When comparing the proportion of mCherry$^+$ ventricular CMs from cryoinjured and control hearts, we observed that the portion of mCherry$^+$ myocardium increased ∼100-fold at 14 days post-injury (dpi) (Figure 1O). We questioned whether *sox10*-derived cells expanded globally in the injured heart or whether there was a distinct contribution to the regenerating myocardium. To do this, we generated a distance distribution map for the *sox10*-derived CMs from the injury site (for injured hearts; Figure 1P) or apical myocardium (for uninjured hearts; Figure 1Q) to the basal myocardium. The closer to the injury area, the greater the contribution of *sox10*-derived CMs (Figure 1P; n = 6). This bias toward an apical region was not detected in uninjured hearts (Figure 1Q; n = 6).

The presence of adult *sox10*$^+$ CMs was confirmed using the line *Tg(−4.9sox10:GFP)^{ba2}* (Carney et al., 2006; Figure S1A). We were able to detect few *sox10*:GFP$^+$ CMs in the ventricle of injured and uninjured hearts (Figures S1B–S1E″; n = 4 hearts). Moreover, RNAScope mRNA detection revealed *sox10* expression in the heart (Figures S1F–S1I″). In uninjured hearts, we found expression both in the atrium (2 out of 3 hearts) as well as in the ventricle (1 out of 3 hearts). In injured hearts, *sox10* signal was detected close to the cortical and trabecular myocardial boundaries, as well as at the borders of the injury area (n = 3 out of 3 hearts). This suggests that *sox10* mRNA increases upon injury or that *sox10*$^+$ cells accumulate at the site of injury. Surprisingly, we did not detect an expansion of *sox10*:GFP$^+$ cells after cardiac injury (Figures S1A–S1E″; n = 4 hearts). The inconsistency between *sox10* mRNA detection and *sox10*:GFP expression in the reporter line might be a

Figure 1. Contribution of *sox10*-Derived CMs to Heart Regeneration

(A) Analysis of *sox10*-derived cells in the adult zebrafish heart. Two 4-OHT pulses were administered to adult *sox10:CreER^{T2};ubb:loxP-GFP-loxP-mCherry* zebrafish between 1 and 3 weeks before heart extraction to induce mCherry in *sox10:CreER^{T2}*-expressing cells. mCherry (red), *sox10* lineage. Anti-MHC marks CMs (green) in uninjured hearts (B–G) or hearts at 14 dpi (I–N).

(B–C″) Cryosections of uninjured hearts fixed 19 days after the last 4-OHT pulse. Upper row, mCherry channel, lower row, merged channels. Arrowheads, mCherry$^+$ CMs; arrows, mCherry$^+$ non-CMs within the atrioventricular valve.

(D–G) Whole-mount views (D) and sections (F and G) of uninjured hearts fixed 11 days after 4-OHT treatment. (D and E) Whole-mount immunostaining. Maximal projection of 352 μm, 44 z planes. (D′–D‴) Maximum projection of zoomed view of boxed area in D (7 μm, 7 z planes). (F and G) Immunostaining on cryosection of an uninjured heart. (F′–F⁗) Zoomed view of boxed area in (F). Images are stitched high resolution acquisitions (9 images stitched together). *sox10*-derived CMs and non-CMs are observed in the subepicardial area of the ventricle. mCherry$^+$ cells in the cortical myocardium (white arrowheads), mCherry$^+$ trabecular CMs (yellow arrowheads).

(H) Analysis of *sox10*-derived cells in the regenerating heart. Two 4-OHT pulses were administered to adult *sox10:CreER^{T};ubb:loxP-GFP-loxP-mCherry* 1 and 3 days after the injury to induce mCherry expression in *sox10:CreER^{T2}*-expressing cells. Hearts were extracted at 14 dpi.

(I and J) Whole-mount view of injured heart at 14 dpi (594 μm, 73 z planes). Shown are the merged (I) and red (J) channel. *sox10*-derived CMs can be observed in the apical region of the heart. (J′–J‴) Zoomed view of boxed area in (J).

(K and L) z stack from heart in I (252 μm, 31 z planes), showing injured area. Image shown in (K) is comprised of four stitched high-resolution acquisitions. Shown are the merged (K) and the red (L) channels. Yellow arrowheads, mCherry$^+$; MHC$^+$ trabecular CMs. White arrowheads, mCherry$^+$; MHC$^+$ cortical CMs.

(M and N) Paraffin sections of injured hearts at 14 dpi. Note the distribution of *sox10*-derived CMs around the IA (yellow arrowheads). Shown are the merged (M) and the red channel (N). Zoomed view of boxed area in (M) is shown in (M′) and (M″). Note cortical (white arrowheads) and trabecular (yellow arrowheads) *sox10*-derived CMs adjacent to the IA.

(O) Percentage of the volume from mCherry$^+$/MHC$^+$ cells relative to all MHC$^+$ cells in uninjured (n = 6) and injured hearts (n = 6) at 14 dpi. The volume of *sox10*-derived CMs expands after injury. Data are mean ± SD; p = 0.0022 (two-tailed non-parametric t test).

(P) The ventricles from whole-mount stained hearts were digitally sectioned in increments of 100 μm starting from the injury site. Shown is the percentage of the volume from mCherry$^+$/MHC$^+$ cells relative to all MHC$^+$ cells within different heart segments. The percentage of mCherry$^+$/MHC$^+$ cells is high near to the injury site and decreases toward more distant ventricular regions (injured hearts, n = 6). Data are mean ± SD; *p < 0.05; ***p < 0.001 (one-way ANOVA test followed by Tukey's post hoc test).

(Q) The ventricle was digitally sectioned in increments of 100 μm starting from the apex. Shown is the percentage of the volume from mCherry$^+$/MHC$^+$ cells relative to all MHC$^+$ cells within different heart segments. The percentage of mCherry$^+$/MHC$^+$ cells is similarly distributed through ventricular regions of the uninjured ventricle (uninjured hearts n = 6). Data are mean ± SD; p > 0.05 (one-way ANOVA followed by Tukey's post hoc test).

4-OHT, 4-hydroxytamoxifen; At, atrium; CI, cryoinjury; CMs, cardiomyocytes; dpi, days post-injury; dpt, days post-treatment; IA, injured area; V, ventricle. Scale bars, 100 μm. See also Figure S1.

consequence of partial silencing of the reporter leading to an incomplete recapitulation of endogenous *sox10* expression. Alternatively, it might indicate that the *sox10*-derived cells in regenerating hearts were descendants from a small subset of *sox10*$^+$ progenitor cells within the uninjured heart that turn off *sox10* expression after cellular expansion and CM differentiation.

Preexistent *sox10*-Derived CMs Contribute to Cardiac Regeneration

To assess whether the increased number of *sox10*-derived CMs is a result of the expansion of a small pool of preexistent *sox10*$^+$ cells, we induced recombination in adult zebrafish before cryoinjury (Figures 2 and S1J–S1T). 4-OHT treatments 2 weeks prior to cardiac injury allowed us to rule out that non-metabolized 4-OHT could be active and induce recombination after injury (Figure 2A). While in controls we again saw only few cells scattered throughout the ventricle, at 7 dpi, we indeed observed *sox10*-derived CMs close to the injury area (Figures 2B–2C′). More *sox10*-derived cells contributed to the ventricle after 7 dpi compared to uninjured hearts (Figure 2D). The percentage of *sox10*-derived CM was higher close to the injury area compared to the basal ventricle (Figure 2E). This preferential distribution of *sox10*-derived CMs toward the apical region was not found in uninjured hearts of siblings (Figure 2E). The proportion of *sox10*-derived CMs significantly expanded upon injury both in the trabecular and cortical myocardium regions (Figure S1S).

We also analyzed the proportion of *sox10*-derived cells at later stages of regeneration to assess if the expansion is transient or whether these cells contribute to the regenerated heart (Figures 2F–2J and S1T). At 14 dpi, *sox10*-derived CMs remained around the injured area (Figures 2F and 2G). Even at 210 dpi, when regeneration is complete (González-Rosa et al., 2011), mCherry$^+$/MHC$^+$ CMs were still detected within the region presumably corresponding to the regenerated myocardium (Figures 2H and 2H′). Similar to the observation when tracing *sox10*-derived cells after cryoinjury, the volume of mCherry$^+$ cells increased over 100-fold after injury when compared with uninjured hearts (Figure 2I). Quantification showed that consistent with the results at 7dpi, the mCherry$^+$/MHC$^+$ myocardial volume was significantly higher in injured hearts than in uninjured hearts at all regeneration stages analyzed (Figures 2J and S1T).

To understand the mechanisms of the accumulation of *sox10*-derived cells at the injury area, we assessed cell proliferation (Figure 3). Recombination was induced 2 weeks before cryoinjury, and bromodeoxyuridine (BrdU) was injected at 6 dpi (Figure 3A). Immunostaining against mCherry to detect the *sox10* lineage, the myocardial marker MHC, and BrdU to label proliferating cells showed the presence of mCherry$^+$/BrdU$^+$ double-positive cells (Figures 3B–3G‴′). Quantification revealed a statistically significant increase of ~30% in the amount of proliferating *sox10*-derived CMs (n = 6) when compared to *sox10*-lineage negative CMs (n = 6) (Figure 3H). We also observed a higher degree of BrdU$^+$ /mCherry$^+$ cells compared to the rest of CMs at later stages of regeneration (Figures 3I–3K). Thus, CMs with an active *sox10* promoter element in the uninjured heart divide at a higher rate than the rest of the CMs within the same anatomical region in response to injury.

Origin of *sox10*-Derived Cells Contributing to Regeneration

Next, we wanted to determine the developmental time point at which this *sox10*$^+$ CM subset with capacity to contribute to heart regeneration appears, as well as elucidate a possible neural crest cell origin. We treated *sox10:CreER*^{T2}*;ubb:Switch* embryos with 4-OHT between 12 and 48 h post-fertilization, the time window of neural crest cell addition to the developing heart (Abdul-Wajid et al., 2018; Cavanaugh et al., 2015; Mongera et al., 2013). We followed individual *sox10:CreER*^{T2}*;ubb:Switch* animals in a longitudinal study (Figure S2A). First, we performed live imaging at 5 days post-fertilization (dpf). The *sox10:CreER*^{T2} line additionally harbors a myocardial reporter cassette, a *myosin light chain 7* (*myl7*) promoter element driving GFP expression in CMs, which was useful to mark myocardial cells. We detected mCherry$^+$/*myl7*:GFP$^+$ in the larval heart, indicating the presence of a subset of CMs derived from *sox10*-expressing cells (Figures S2B and S2C; n = 7). As reported for *sox10:Cre* genetic tracing (Abdul-Wajid et al., 2018), using the *sox10:CreER*^{T2} line, the proportion of *sox10*-derived cells in the trabecular myocardium was higher than in the compact myocardium, which at this stage is composed exclusively of the primordial layer (Gupta and Poss, 2012; Figure S2D). After live imaging, larvae were grown separately to adulthood to follow the fate of mCherry$^+$ cells. In the adult, we again detected mCherry$^+$ cell clusters, showing that embryonic *sox10*-derived cells contribute to the adult heart (Figures S2E and S2F; n = 7) and confirming observations using a non-inducible *sox10:Cre* line (Abdul-Wajid et al., 2018). Embryonic *sox10*-derived cells contributed to 5% of the total ventricular volume of the adult heart (Figure S2G). Indeed, immunofluorescence staining and fluorescence activated cell (FAC) sorting confirmed that most of the mCherry$^+$ cells were also *myl7*:GFP$^+$ and MHC$^+$ and thus CMs (Figures S2H–S2L). We observed mCherry$^+$ cells in the ventricle and atrium in most of the animals analyzed. The mCherry signal was particularly evident in the basal and medial portion of the ventricle, presumably due to a higher cell density in these regions (Figure S2M; n = 19 hearts analyzed).

To determine whether the embryonic *sox10*-derived population expanded in response to injury, we cryoinjured ventricles from adult *sox10:CreER*^{T2}*;ubb:Switch* zebrafish recombined during embryogenesis and compared the percentage of mCherry$^+$ cells in injured and uninjured hearts (Figure 4A). mCherry$^+$ cells were detected in a similar proportion in uninjured hearts (Figures 4B–4E; n = 12) and hearts at 14 dpi (Figures 4F–4J, n = 9; and Figure 4K, n = 5). While a tendency of higher amount of mCherry$^+$ signal was observed within the injury area, the increase did not reach significance, eventually due to the high degree of heterogeneity in injury response. Similarly, in uninjured hearts, no apicobasal region was identified with a preferred contribution of mCherry$^+$ cells (Figure 4L; n = 5). These results imply that in the adult heart, CMs derived from *sox10*$^+$ embryonic cells do not expand in response to injury and are not preferentially contributing to myocardium regeneration.

To further fine-tune the characterization of *sox10*-derived cells, we performed 4-OHT recombination in juveniles. We used 9-week-old *sox10:CreER*^{T2}*;ubb:Switch* as well as *sox10:CreER*^{T2cn17} crossed to *vmhcl:loxP-tagBFP-loxP-mCherry-NTR*

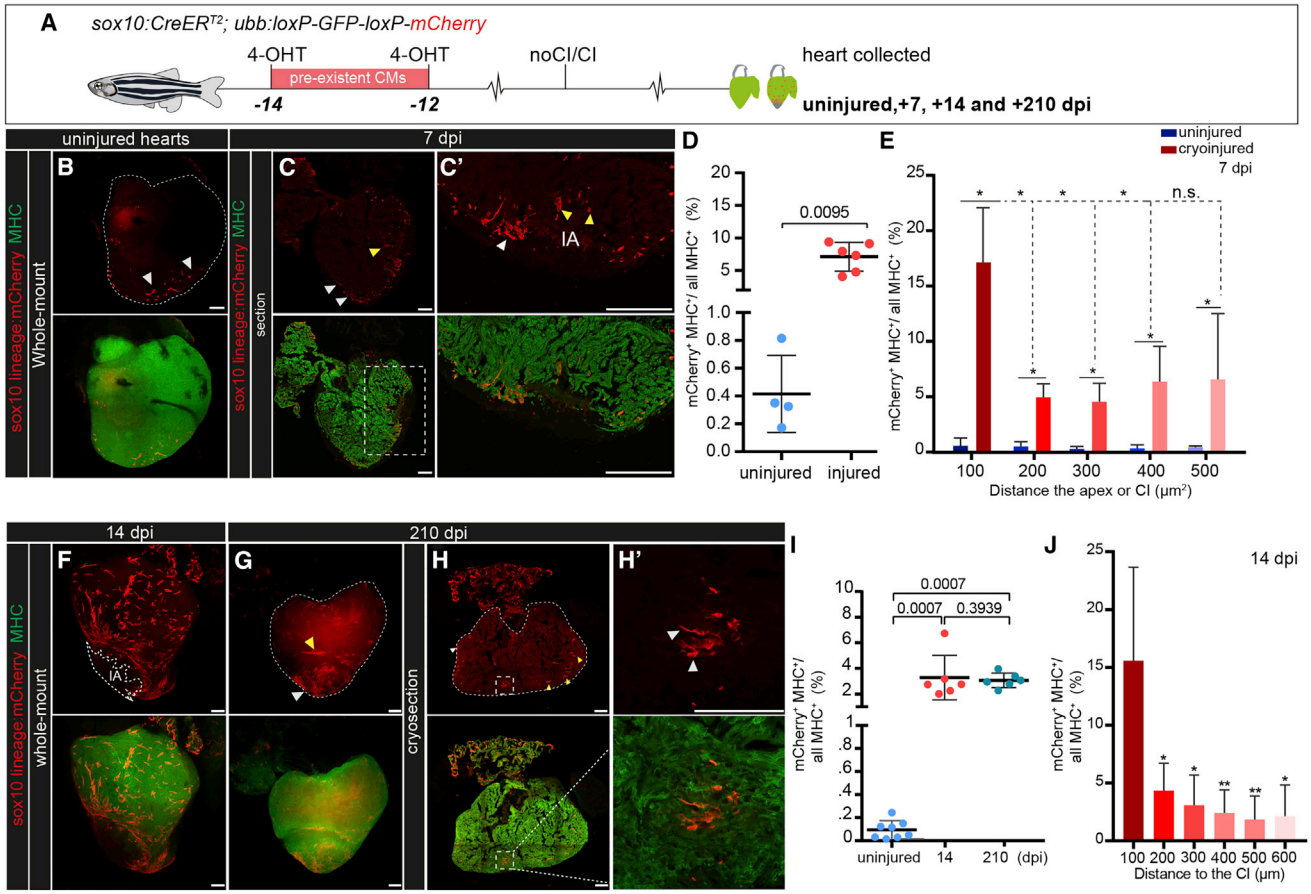

Figure 2. Preexistent *sox10*-Derived CMs Expand at the Injury Area and Contribute to Cardiac Regeneration

(A) Adult *sox10:CreER^{T2};ubb:loxP-GFP-loxP-mCherry* zebrafish were treated with 4-OHT on days 14 and 12 before cryoinjury. Hearts were fixed at 7, 14, or 210 dpi and processed for immunostaining with anti-mCherry$^+$ (red, *sox10*-derived cells) and anti-MHC (green, myocardium).

(B) Whole mounts of uninjured hearts. Upper row, mCherry channel; lower row, myosin heavy chain (MHC) and mCherry merged channels. Arrowheads indicate *sox10*-derived cells.

(C and C′) Cryosection of an injured heart at 7 dpi. *sox10*-derived CMs are detected near the injured area (IA) and subepicardial regions of the myocardium. White arrowheads indicate mCherry$^+$ CMs in the cortical myocardium, and yellow arrowheads indicate mCherry$^+$ CMs in the trabecular myocardium.

(D) Quantification of the proportion of *sox10*-derived CMs in uninjured (n = 4) and injured hearts (n = 6) at 7 dpi. Each dot represents the value from one heart. Data are mean ± SD; p = 0.0095 (two-tailed non-parametric t test).

(E) Quantification of the distribution of ventricular mCherry$^+$ CMs on uninjured and cryosectioned hearts at 7 dpi. The ventricle was digitally divided into increments of 100 μm starting from the injury site in injured hearts or apex in uninjured hearts. Shown is the percentage of the mCherry$^+$/MHC$^+$ area relative to the whole MHC$^+$ area within different heart segments. The percentage of mCherry$^+$/MHC$^+$ is high near the IA and decreases toward ventricular regions distant from the IA (injured hearts n = 5; uninjured hearts, n = 4). Dashed lines represent statistical differences, and red bars represent injured hearts. The percentage of mCherry$^+$/MHC$^+$ cells is higher in every region of the injured heart ventricle (red bars) compared to uninjured heart ventricles (blue bars). Data are mean ± SD; *p < 0.05 (two-tailed non-parametric t test).

(F) Whole-mount image of a heart at 14 dpi. *sox10*-derived CMs are distributed around the IA and distant part of the ventricle.

(G–H′) Whole-mount view (G) and cryosections (H and H′) of regenerated hearts at 210 dpi. *sox10*-derived CMs can be observed in the apical region of the heart. White arrowheads show mCherry$^+$ CMs in the cortical myocardium, and yellow arrowheads show mCherry$^+$ CMs in the trabecular myocardium. Image shown in (H) is comprised of nine stitched high-resolution acquisitions.

(I) Quantification of the percentage of mCherry$^+$ CMs in uninjured cardiac ventricles compared to ventricles at 14 and 210 dpi (whole-mount immunostained hearts). Shown are measurements of individual hearts (dots) as well as mean ± SD (two-tailed non-parametric t test; uninjured, n = 8; 14 dpi, n = 6; 210 dpi, n = 6).

(J) Quantification of the distribution of mCherry$^+$ CMs in whole mount immunostained hearts. Distance calculation as shown in (E). Data are mean ± SD. *p < 0.05; **p < 0.01 (two-tailed non-parametric t test; n = 6).

At, Atrium; dpi, days post-injury; IA, injured area; MHC, myosin heavy chain; V, ventricle. Scale bars represent 100 μm (except for C′, where scale bars represent 200 μm). See also Figure S1.

(vmBRN), a line that allows to specifically trace recombined *vmhcl*-expressing ventricular CMs by mCherry expression (Sánchez-Iranzo et al., 2018). After recombination, animals were raised and cryoinjured at 17 weeks of age (Figure 5A). We observed an increase in the *sox10*-derived cell area after injury (Figures 5B–5S). This was most evident when observing

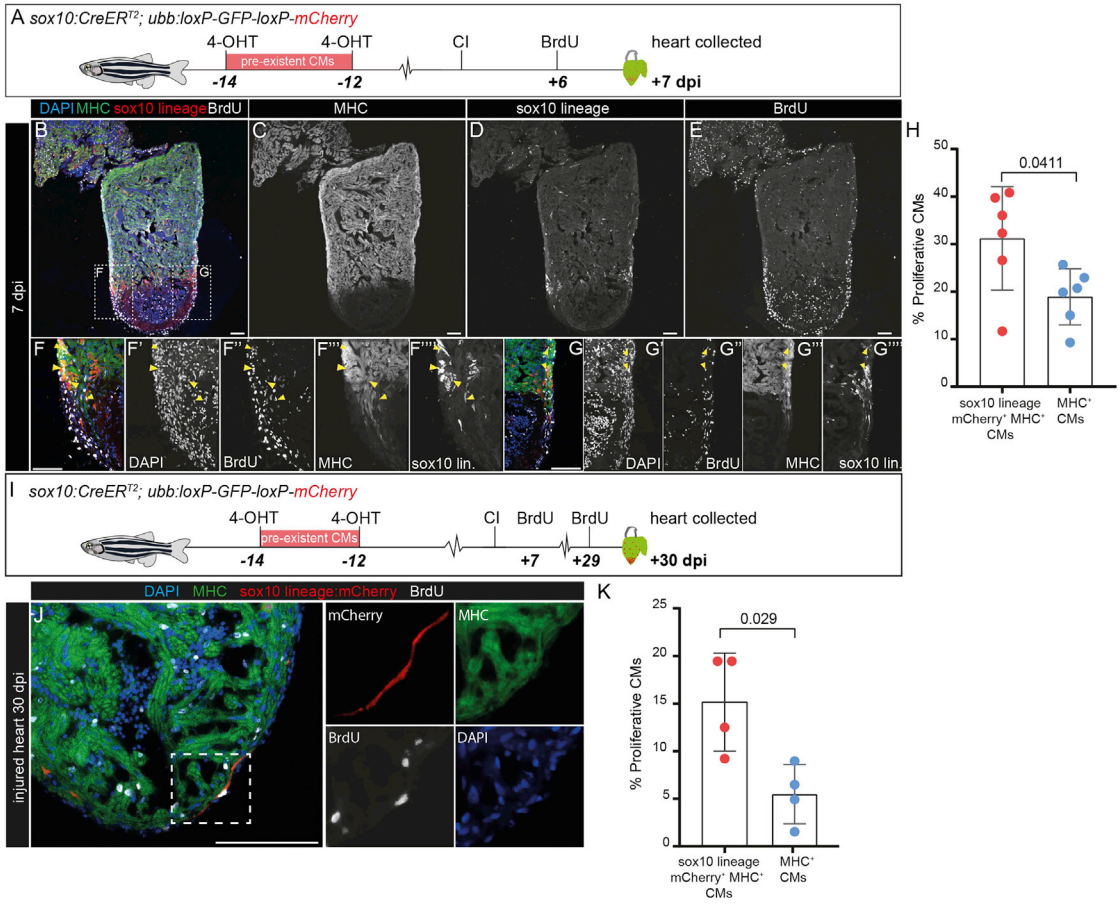

Figure 3. Proliferation of *sox10*-Derived CMs

(A) Assessment of the proliferation index of *sox10*-derived CMs. Two pulses of 4-OHT were administered 14 and 12 days before the injury. BrdU was added at 6 dpi, and hearts were collected at 7 dpi.

(B–E) Heart section immunostained with anti-BrdU (white), anti-mCherry (red, *sox10* lineage), and MHC (green). Nuclei were counterstained with DAPI (blue). Shown are merged channels (B), as well as single channels for MHC (C), mCherry (D), and BrdU (E) staining.

(F–G‴′) Zoomed views of boxed regions in (B). Yellow arrowheads, mCherry$^+$, BrdU$^+$, MHC$^+$ triple-positive cells. Shown are merged channels (F and G), as well as single channels for DAPI (F′ and G′), BrdU (F″ and G″), MHC (F‴ and G‴) and mCherry (F‴′ and G‴′).

(H) Quantification of mCherry$^+$, BrdU$^+$, MHC$^+$ triple-positive cells versus all BrdU$^+$, MHC$^+$ double-positive cells in the 100 μm IA border zone. Shown are values for individual hearts as well as mean ± SD. *p < 0.05 (two-tailed non-parametric t test; n = 6).

(I) Assessment of proliferation at late stages of regeneration. 4-OHT was added at −12 and −14 days to *sox10:CreER^{T2};ubb:loxP-GFP-loxP-mCherry* zebrafish before cryonjury. BrdU was added at 6 and 29 dpi. Hearts were collected at 30 dpi.

(J) Immunofluorescence staining on heart at 30 dpi. MHC, green; mCherry, red; BrdU, white; nuclei are counterstained with DAPI (blue). Shown are merged images and single channels, and the zoomed region is highlighted with dotted lines.

(K) Quantification of BrdU$^+$ CMs at 30 dpi. Data are mean ± SD (p = 0.029; two-tailed non-parametric t test).

At, Atrium, dpi, days post-injury; IA, injured area; MHC, myosin heavy chain; V, ventricle. Scale bars, 100 μm.

whole-mount hearts (Figures 5D and 5M). *sox10*-derived CMs were predominantly observed in the subepicardial regions of the ventricle (Figures 5H–5J and 5Q–5S). Quantification of mCherry signal within the ventricle indicated a difference between uninjured and injured groups, which did not reach statistical significance (Figure 5T). Also, no overall expansion of mCherry$^+$ cells could be observed by quantification on the sectioned hearts (Figure 5U). However, we observed that within the different apicobasal regions, the proportion of mCherry$^+$ cells was clearly increased when compared to uninjured hearts (Figure 5V). Similar to results obtained in adults, mCherry$^+$ cells accumulated close to the injury site, suggesting that the *sox10*$^+$ population is already present in the juvenile heart. Importantly, control experiments, with no 4-OHT, yielded no recombination, and the hearts were completely devoid of mCherry expression, both in juveniles and adults (Figures 5W–5Y). Thus, with *sox10:CreER^{T2}*, we are fully controlling recombination events and can therefore faithfully trace the fate of cells with active *sox10:CreER* ^{T2} expression at the time of 4-OHT addition.

Collectively, these results show that *sox10:CreER^{T2}* fate mapping enables the detection of a subset of CMs present

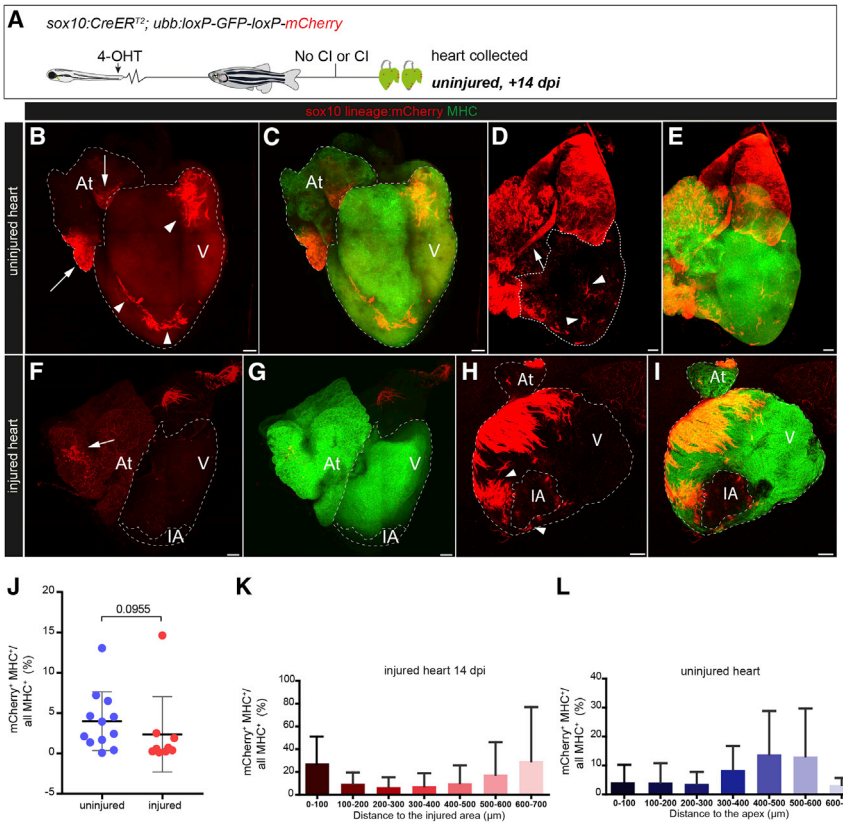

Figure 4. Embryonic *sox10*-Derived CMs Do Not Expand after Cryoinjury

(A) 4-OHT was administered to *sox10:CreER^{T2}; ubb:loxP-GFP-loxP-mCherry* zebrafish during embryogenesis (12–48 h post-fertilization), and adult uninjured hearts or hearts at 14 dpi were collected and imaged.

(B–I) Maximal intensity projection of a confocal z stack through an immunostained heart. *sox10*-derived cells are mCherry$^+$ (red). The whole myocardium is MHC$^+$ (green). mCherry$^+$ cells are present in the ventricle (arrowheads) and atrium (arrows). Shown are merged channel views (C, E, G, and I) as well as mCherry (red) channel only (B, D, F, and H).

(J) Relative volume of embryonic *sox10*-derived CMs (mCherry$^+$/ MHC$^+$) compared to all CMs (MHC$^+$) in uninjured (n = 12) and injured hearts at 14 dpi (n = 9). Shown are values from individual hearts as well as mean ± SD; p = 0.0955 (two-tailed non-parametric t test).

(K and L) Quantification of the distribution of mCherry$^+$ CMs in whole mount immunostained hearts. The ventricle was digitally sectioned in increments of 100 μm starting from the injury site or apex. Shown is the relative volume from mCherry$^+$/ MHC$^+$ cells versus all MHC$^+$ cells within different heart segments. The amount of mCherry$^+$/MHC$^+$ cells does not differ between segments (one-way ANOVA). n = 5 hearts for 14 dpi (K) and n = 5 for uninjured condition (L). The atrium, ventricle, and injury area are outlined by dotted lines.

4-OHT, 4-hydroxytamoxifen; At, atrium; dpi, days post-injury; IA, injured area; CI, cryoinjury; CMs, cardiomyocytes; V, ventricle. Scale bars, 100 μm. See also Figure S2.

in the adult heart that expands in response to injury and contributes preferentially to myocardial regeneration in the zebrafish.

sox10-Derived CMs Reveal a Specific Gene Signature

To investigate if *sox10*-derived CMs differ in their gene expression profile compared to other CMs, we performed transcriptome analysis (Figures 6A and 6B). To make the characterization specific for the myocardium, we used the *sox10:CreER^{T2}; vmBRN* line, in which upon 4-OHT-induced recombination, *sox10*-derived CMs express mCherry and the rest of the ventricular CMs express blue fluorescent protein (BFP). Two pulses of 4-OHT were administered 2 weeks before injury and 3 weeks before heart dissection. mCherry$^+$, BFP$^+$, and double-positive mCherry$^+$/BFP$^+$ CMs were FAC sorted from *sox10:CreER$^{T2\ cn17}$;vmBRN* uninjured hearts and hearts at 7 dpi and processed for RNA sequencing (RNA-seq). For bioinformatics analysis, we compared mCherry$^+$ (comprising all samples that were mCherry$^+$ or mCherry$^+$/BFP$^+$) with mCherry$^-$ (comprising samples that were only BFP$^+$).

In uninjured hearts, 101 genes were upregulated and 129 genes were downregulated in *sox10*-derived (mCherry$^+$) CMs compared to the rest of the ventricular CMs (mCherry$^-$) (Figures 6A and 6B; Table S1). Gene enrichment analysis of mCherry$^+$ and mCherry$^-$ transcriptomic profiles in uninjured hearts revealed several metabolic differences between these two groups, including changes in oxidative phosphorylation and nucleic acid metabolism (Figures 6C, 6D, and S3; Table S1).

Notably, when comparing mCherry$^+$ and mCherry$^-$ groups after injury, *sox10*-derived cells were transcriptionally more active; 415 genes were upregulated in mCherry$^+$ CMs, while only 30 genes were upregulated in mCherry$^-$ CMs (Figure 6B; Table S2). Importantly, *sox10* mRNA was significantly upregulated in mCherry$^+$ CMs from injured hearts at 7 dpi, showing that the *sox10:CreER^{T2}* line allows tracing of endogenous *sox10*-expressing cells. The genes encoding the T-box transcription factors *tbx20* and *tbx5a* were among the genes upregulated in *sox10*-derived CMs (Figure 6B; Table S2). These genes were previously shown to be expressed in CM populations involved in heart regeneration (Sánchez-Iranzo et al., 2018) and play an active role in this process (Grajevskaja et al., 2018; Xiang et al., 2016).

Gene enrichment analysis in injured conditions for mCherry$^+$ and mCherry$^-$ CMs showed that Gene Ontology (GO) biological processes related to negative regulation of the cell cycle were inhibited in mCherry$^+$ CMs. This suggests that mCherry$^+$ CMs have a pro-regenerative profile (Figures 6E–6G and S3; Table S2). Furthermore, mCherry$^+$ CMs were enriched for pathways involved in myocardial growth, including CM differentiation, cardiac cell development, and cardiac muscle contraction (Figures 6E–6G; Table S2). This result is consistent with a role for *sox10*-derived CMs in rebuilding the lost myocardium.

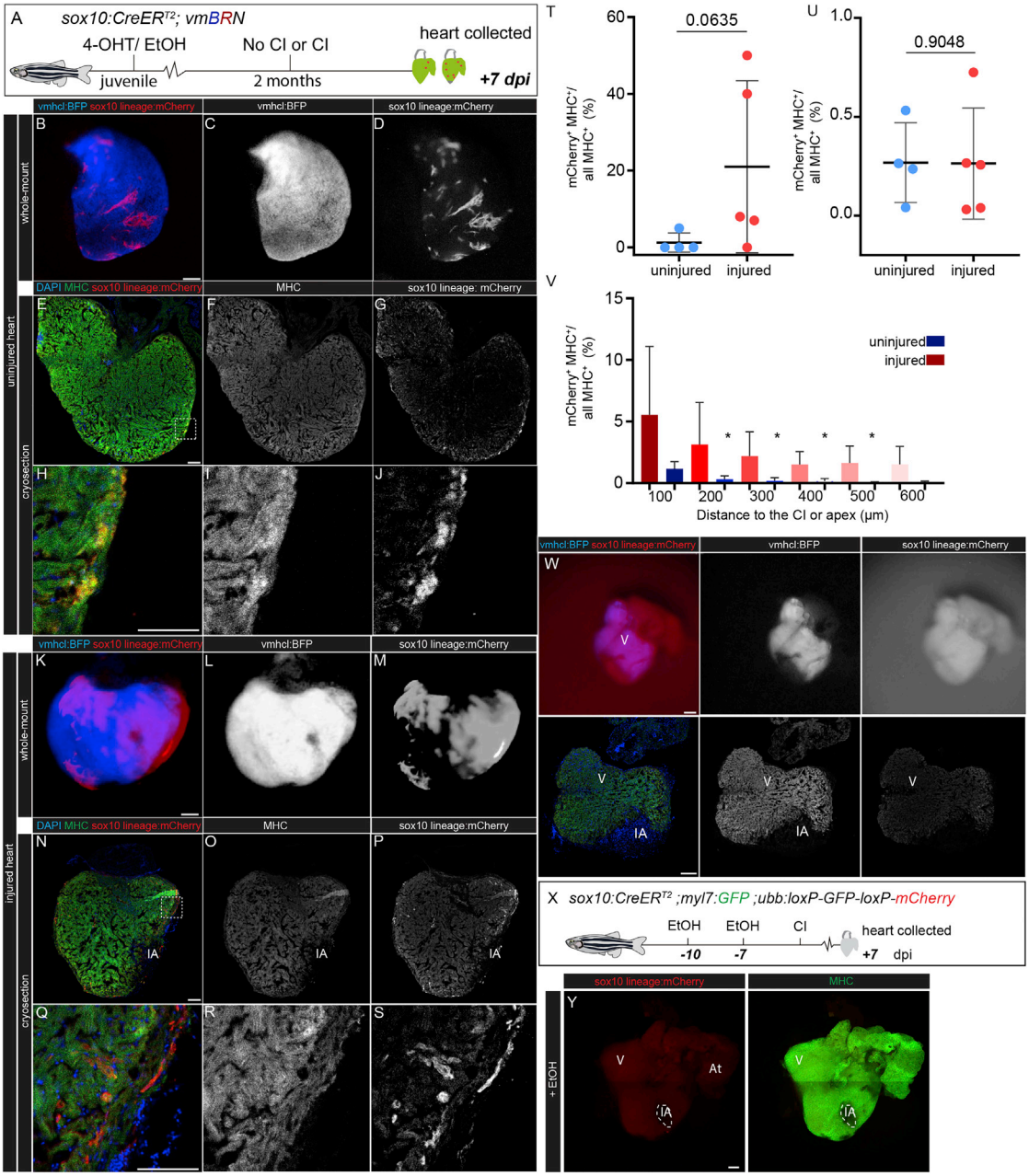

Figure 5. Fate Mapping of Juvenile *sox10*$^+$ Cells and Evidence of Non-leaky *sox10:CreER*^{T2} Activity

(A) 4-OHT was administered to *sox10:CreER*^{T2}*; vmhcl:loxP-tagBFP-loxP-mCherry-NTR* (*sox10:CreER*^{T2}; *vmBRN*) zebrafish during juvenile stage (9 weeks post-fertilization), and adult uninjured hearts or hearts at 7 dpi were collected and imaged.

(B–D) Fluorescence stereomicroscope acquisition of a dissected uninjured heart showing *sox10*-derived CMs in red (mCherry$^+$) and other ventricular CMs in blue (*vmhcl*:BFP$^+$). (B) Merged channels (B), blue channel (C), and red channel (D) are shown.

(E–J) Cryosection of an uninjured heart. Shown are merged (E) as well as single green (MHC$^+$ cells; F) and red (mCherry$^+$ cells; G) channels. (H–J) Zoomed views of boxed region in (E). Again, merged (H) as well as single green (I) and red (J) channels are shown. *sox10*-derived CMs (mCherry$^+$) are detected near the sub-epicardial regions of the myocardium.

(K–M) Fluorescence stereomicroscope acquisition of a dissected injured heart showing *sox10*-derived cells in red (mCherry$^+$) and ventricular CMs in blue (*vmhcl*:BFP$^+$). Merged channels (K), blue channel (L), and red channel (M) are shown.

(N–S) Cryosection of an injured heart at 7 dpi. *sox10*-derived CMs are detected near the subepicardial regions and close to the injured area. Shown are merged (N) as well as single green (MHC$^+$ cells; O) and red (mCherry$^+$ cells; P) channels.

(Q–S) Zoomed views of boxed region in (N). Shown are merged and single channels of MHC and mCherry signal. Again, merged (Q) as well as single green (R) and red (S) channels are shown.

(legend continued on next page)

We next analyzed if mCherry$^+$ cells respond equally to an injury as other CMs. For this, we compared on the one hand the changes in gene expression of mCherry$^+$ CMs in injured with uninjured hearts (Figure S4) and on the other the changes in gene expression of mCherry$^-$ CMs between both conditions (Figure S5). Upon injury, mCherry$^+$ cells upregulated 767 genes, and only 26 genes were downregulated (Figure S4C; Table S3). Thus, overall, mCherry$^+$ CMs respond to injury with an increase in gene expression. Biological processes related to cell proliferation, cell motility, and response to injury were enriched in mCherry$^+$ CMs upon cryoinjury (Figure S4D; Table S3). Ingenuity pathway analysis (IPA) further confirmed the enrichment of canonical pathways related to proliferation in mCherry$^+$ CMs of injured hearts (Figure S4E; Table S3).

When we analyzed the changes in gene expression of the rest of the CMs (mCherry$^-$) in response to injury, we observed fewer differentially expressed genes (DEGs) than those detected for mCherry$^+$ cells (Figure S5; Table S4). This indicated that *sox10*-derived cells reactivate gene expression to a larger extent when compared to the rest of the CMs.

Altogether, these data indicate that *sox10* promoter expression defines a group of myocardial cells in the adult uninjured zebrafish heart with a unique gene expression signature and pro-regenerative transcriptomic profile in response to injury.

sox10$^+$ Cells Are Necessary for Cardiac Regeneration

The accumulation of *sox10*-derived cells in the regenerated myocardium strongly suggests that these cells contribute to the replacement of injured myocardium. To determine the function of this population during heart regeneration, we genetically ablated *sox10*-derived cells using the transgenic line *sox10:CreER^{T2};β-actin:loxP-mCherry-loxP-DTA* (Wang et al., 2011), which allows cell ablation upon diptheria toxin (DTA) overexpression. We administered 4-OHT to adults 3 days and 1 day before cryoinjury (Figure S6A). At 21 dpi, the injured area was larger in *sox10*$^+$-cell-depleted animals than in the control group (Figures S6B–S6D; n = 13 without 4-OHT and n = 8 with 4-OHT), suggesting that *sox10*-derived cells are necessary for heart regeneration. There was no significant reduction in animal survival or cardiac function in *sox10*-cell ablated animals (Figures S6E–S6I; n = 6). During development, *sox10*-derived cells contribute to the peripheral nervous system, which plays an important role in heart regeneration (Mahmoud et al., 2015; White et al., 2015). Thus, the impaired regeneration in animals with *sox10*-ablated cells might be a consequence of compromised cardiac innervation. Yet, the *β-actin* promoter used in the transgenic line has been reported to be strongly expressed in CMs but weak in other cardiac cells (Kikuchi et al., 2010). Nonetheless, we assessed a possible change in innervation upon induced Diphtheria toxin A (iDTA)-based *sox10*$^+$ cell ablation by anti-tyrosine hydroxylase immunostaining. This experiment yielded no evidence of a reduction in innervation in *sox10*$^+$ cell ablated hearts when compared to controls (Figures S6J–S6N), suggesting that the ablation of *sox10*-derived CMs is responsible for the phenotype.

For confirmation, we genetically ablated *sox10*-derived cells in ventricular CMs using *sox10:CreER$^{T2\ cn17}$;vmBRN* zebrafish (Figure 7A). With this double transgenic line, ventricular *sox10*$^+$-derived CMs can be genetically ablated upon addition of metronidazole (Mtz), which induces cell death in nitroreductase (NTR)-expressing cells (Curado et al., 2008; Figure 7A). We ablated mCherry$^+$ cells 1 week before cryoinjury and confirmed the efficiency of ablation by comparing the amount of mCherry$^+$ cells with Mtz-nontreated animals (Figures 7B and 7C; n = 26 treated and 20 untreated). A significant difference in the amount of *sox10*-derived CMs could be observed between untreated (n = 5) and treated (n = 8) adult zebrafish (Figure 7D), confirming the efficiency of ablation. Consistent with the results using the DTA ablation model, the survival rate of the different groups was similar (Figure 7E). To assess if loss of adult *sox10*-derived ventricular CMs affects heart regeneration after cryoinjury, we collected hearts at 30 dpi and assessed fibrotic tissue deposition (Figures 7F–7H). Fish in which ventricular *sox10*-derived CMs had been ablated revealed a persistent fibrotic scar and a larger injury area compared to the control groups *sox10:CreER$^{T\ cn172}$;vmBRN* without Mtz administration and *sox10:CreER$^{T2\ cn17}$;ubb:loxP-mCherry* with Mtz (Figures 7F–7I). This indicates that ablation of the small pool of *sox10*-derived ventricular CMs in the uninjured adult zebrafish heart, comprising less than 1% of total myocardial volume, affects subsequent heart regeneration upon cryoinjury.

DISCUSSION

CMs can proliferate in the adult zebrafish (Wills et al., 2008), and this can represent a basis for the high regenerative capacity

(T and U) Percentage of juvenile *sox10*-derived CMs area (mCherry$^+$/MHC$^+$) compared to the area of all myocardial cells (MHC$^+$) in uninjured (n = 4) and injured hearts at 7 dpi (n = 5). (T) Analysis performed on whole-mount images as shown in (B) and (K); (U) analysis performed on sectioned hearts as shown in (E) and (N). Shown are data for individual hearts as well as mean ± SD (two-tailed non-parametric t test).

(V) Quantification of *sox10*-derived cells in different apicobasal regions in injured and uninjured hearts. Data are mean ± SD. Statistical testing was performed using one-way ANOVA followed by Tukey's honest significant difference test. *$p < 0.05$ when comparing percentage between injured at 100 μm with uninjured at 200–600 μm.

(W) *sox10:CreER^{T2}; vmBRN* zebrafish as shown in (K)–(M) but without 4-OHT treatment. Note the lack of mCherry$^+$ cells in whole-mount views (upper row) and on sections (lower row) (n = 2).

(X) EtOH was administered to *sox10:CreER^{T2};ubb:loxP-GFP-loxP-mCherry* zebrafish 10 and 7 days before injury, and hearts at 7 dpi were collected and imaged (n = 3).

(Y) Maximal intensity projection of a confocal z stack through a heart from condition as described in (X). *sox10*-derived cells are mCherry$^+$ (red). The whole myocardium is MHC$^+$ (green). Shown are merged and single channels. mCherry$^+$ cells could not be detected. Image shown is comprised of nine stitched high-resolution acquisitions.

4-OHT, 4-hydroxytamoxifen; At, atrium; CI, cryoinjury; CMs, cardiomyocytes; dpi, days post-injury; EtOH, ethanol; IA, injured area; V, ventricle. Scale bar, 50 μm. See also Figure S2.

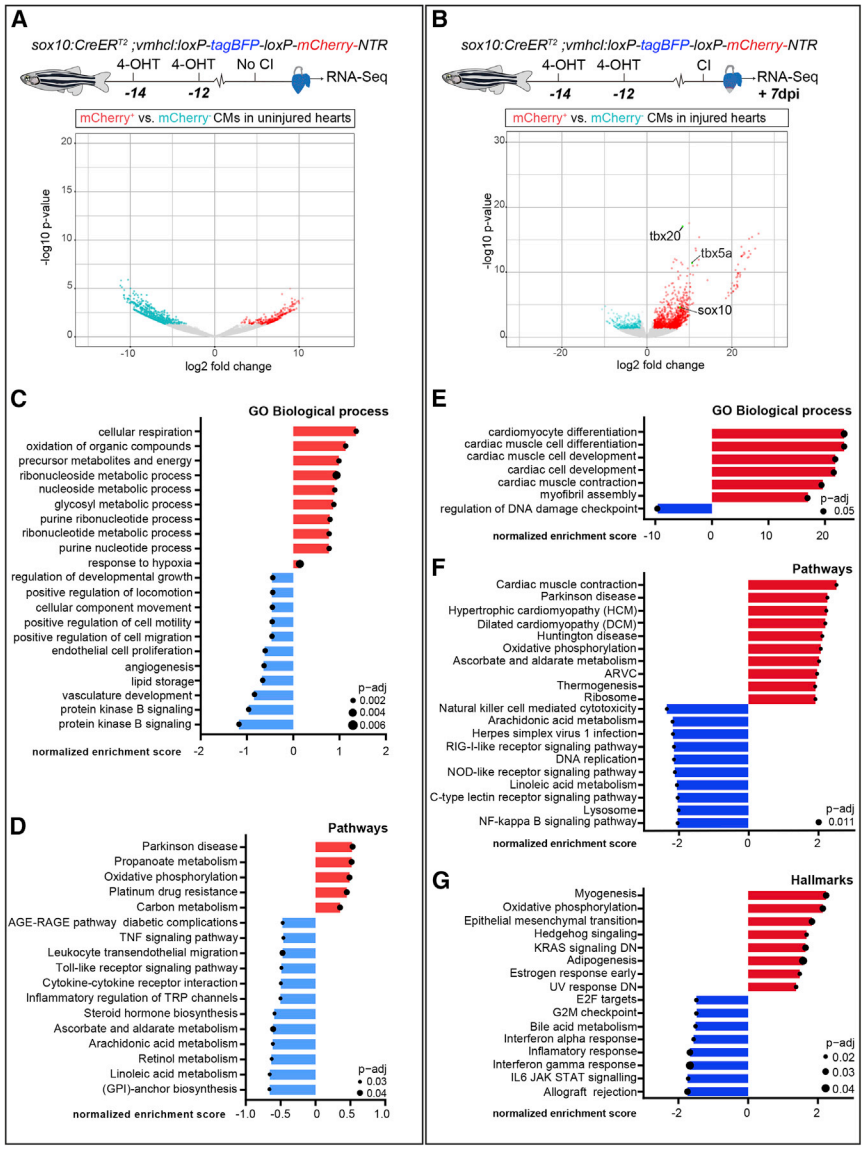

Figure 6. *sox10*-Derived CMs Reveal a Specific Transcriptome Signature

sox10:CreER^{T2};vmhcl:loxP-tagBFP-loxP-mCherry-NTR zebrafish were treated with 4-OHT. A group of zebrafish was cryoinjured and collected at 7dpi and a control group was left uninjured. Hearts were disaggregated, *sox10*-derived CMs (mCherry^{+}) and the rest of the CMs of the heart (mCherry^{-}) were FAC sorted, and RNA-seq was performed on 26 samples consisting of 20 CMs each.

(A and B) Recombination and collection were carried out either on uninjured hearts (A) or hearts at 7 dpi (B). (A) Volcano plots representing differentially expressed genes (DEGs) in mCherry^{+} and mCherry^{-} CMs from uninjured (A) or 7 dpi (B) hearts. DEGs upregulated in mCherry^{-} CMs are shown in blue, and DEGs upregulated in mCherry^{+} CMs in red. These genes had an adjusted p value (adjp) $\leq$ 0.05 and a log2 fold change (LFC) $\geq$2. Genes with a false discovery rate (FDR) $\geq$0.05 are represented in gray. Note the high number of DEGs upregulated in mCherry^{+} cells at 7 dpi. Some differentially expressed genes previously linked to regeneration as well as *sox10* are highlighted.

(C) Biological processes differentially enriched in mCherry^{+} versus mCherry^{-} CMs from uninjured hearts (source for analysis, DEG list).

(D) Pathway analysis using gene enrichment analysis (GSEA) of genes with LFC $\geq$2 present in mCherry^{+} and mCherry^{-} CMs of uninjured hearts. Representative biological processes were plotted and ordered according to the normalized enrichment score. *Z* score represents whether a specific function is increased or decreased. Red bar, enriched in mCherry^{+} CMs; blue bar, enriched in the rest of the CMs.

(E) Biological processes differentially enriched in mCherry^{+} versus mCherry^{-} CMs from injured hearts (source for analysis, DEG list).

(F and G) Pathway analysis (F) and hallmarks (G) using GSEA of genes with LFC $\geq$2 present in mCherry^{+} and mCherry^{-} CMs of injured hearts. Representative biological processes were plotted and ordered according to the normalized enrichment score. *Z* score represents whether a specific function is increased or decreased. Red bar, enriched in mCherry^{+} CMs; blue bar, enriched in the rest of the CMs.

4-OHT, 4-Hydroxytamoxifen; CI, cryoinjury; dpi, days post-injury; dpt, days post-treatment; GO, Gene Ontology. See also Figures S3–S5 and Tables S1, S2, S3, and S4.

observed in the injured heart. Although little is known about CM populations that contribute to regeneration, studies showed that they activate *gata4* and *ctgfa* regulatory elements in response to injury (Kikuchi et al., 2010; Pfefferli and Jaźwińska, 2017). Recent clonal analysis studies using pan-myocardial lineage tracing have suggested that distinct CM subsets can contribute to heart regeneration in the zebrafish as well as mouse (Gupta et al., 2013; Sereti et al., 2018). Here, we report genetic fate mapping with a specific promoter element of preexistent CMs, which are present in the adult heart and expand more than the rest of the CMs in response to injury. Our study suggests that this small *sox10*-derived CM population is essential for regeneration, since its genetic ablation prior to cryoinjury impairs cardiac regeneration. Unfortunately, it was technically not possible to perform an ablation of an equally small random CM population. Thus, we could not fully evaluate if the effect on regeneration was specific to of the effect due to ablation of the *sox10*-derived CM population.

Adult neural crest stem cells were proposed as the source of progenitor cells during adult pigment cell regeneration in the zebrafish (Iyengar et al., 2015). Moreover, in rodents, neural crest stem cells were suggested to participate in repair mechanisms after myocardial infarction (Tamura et al., 2016). A neural crest cell origin of the *sox10*$^{+}$ population contributing to heart regeneration is plausible but should be confirmed with genetic fate mapping using additional neural crest marker

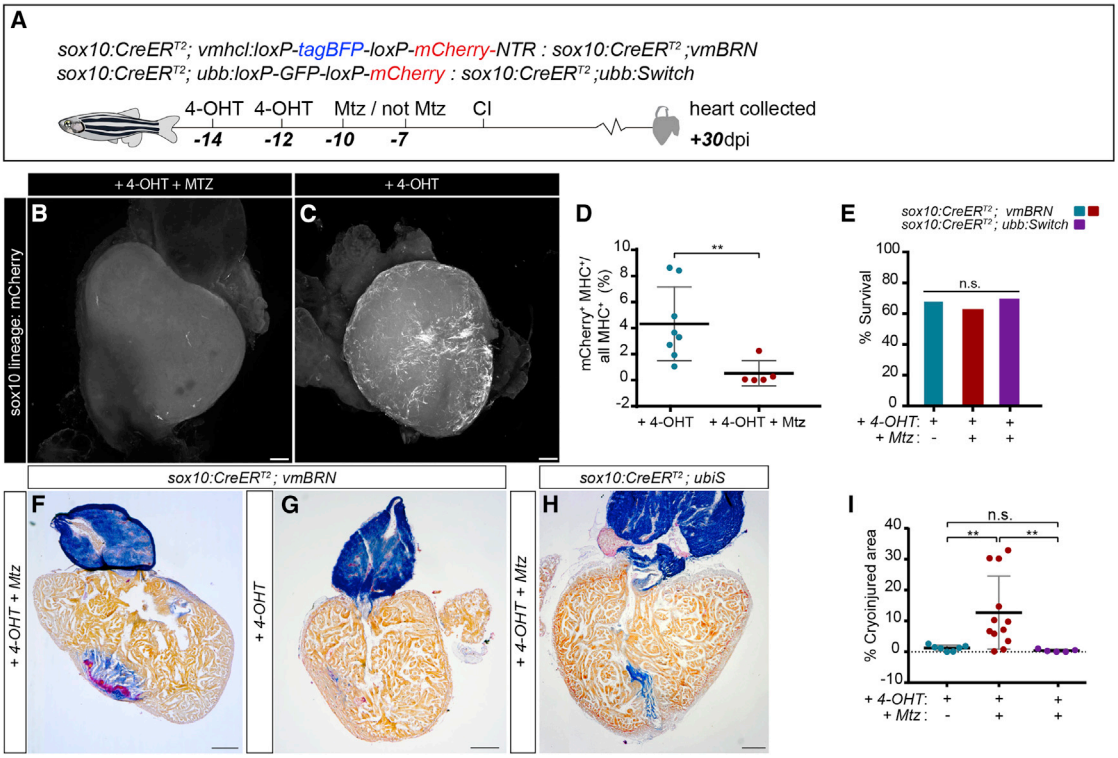

Figure 7. Genetic Ablation of *sox10*$^+$ CMs Impairs Cardiac Regeneration

(A) *sox10:CreER*^{T2}*;vmBRN* or *sox10:CreER*^{T2}*;ubb:Switch* zebrafish were treated with 4-OHT 14 and 12 days before cryoinjury. They were treated with Mtz on days 10 and 7 before injury. A control group of *sox10:CreER*^{T2}*;vmBRN* was not treated with Mtz. Cryoinjured hearts were collected at 30 dpi.

(B and C) Whole-mount view of a confocal 3D projection of z stacks through a *sox10:CreER*^{T2}*;vmBRN* heart after 4-OHT and with (B) or without (C) Mtz treatments and 30 dpi.

(D) Percentage of the volume from mCherry$^+$ CMs relative to all CMs: mCherry$^+$; myosin heavy chain (MHC)$^+$ versus all MHC$^+$ cells ($p = 0.006$; two-tailed non-parametric t test).

(E) Survival rate of animals from the different groups as described in (A). No difference in mortality was observed among groups according to a Fisher's exact test ($p = 1.000$).

(F–H) AFOG histological staining on sagittal sections of cryoinjured hearts at 30 dpi. (F) 4-OHT- and Mtz-treated *sox10:CreER*^{T2}*;vmBRN* heart section. (G) 4-OHT-treated *sox10:CreER*^{T2}*;vmBRN* heart section. (H) 4-OHT- and Mtz-treated *sox10:CreER*^{T2}*;ubb:Switch* heart section.

(I) Quantification of IA in the three conditions shown in (F-H). IA versus total ventricular myocardial area was measured. Shown are values for individual hearts as well as mean ± SD (statistical analysis by non-parametric t test: *sox10:CreER*^{T2}*;vmBRN* Mtz-treated versus *sox10:CreER*^{T2}*;vmBRN* Mtz-untreated, $p = 0.0078$; *sox10:CreER*^{T2}*;vmBRN* Mtz-treated versus *sox10:CreER*^{T2}*;ubb:Switch* Mtz-treated, $p = 0.0072$; *sox10:CreER*^{T2}*;vmBRN* Mtz-untreated versus *sox10:CreER*^{T2}*;ubb:Switch* Mtz-treated, $p = 0.1020$).

4-OHT, 4-hydroxytamoxifen; At, atrium; CI, cryoinjury; dpi, days post-injury; IA, injured area; Mtz, Metronidazole V, ventricle. Scale bars represent 100 μm (B and C) and 200 μm (F–H). See also Figure S6.

genes. Alternatively, the zebrafish heart might harbor a small pool of *sox10*$^+$ CMs that efficiently expand in response to cryoinjury. It will be interesting to elucidate if such an expansion also occurs in other injury setups such as ventricular resection or genetic ablation. Adult *sox10*$^+$ CMs reveal a unique gene signature both in uninjured hearts and upon injury. Interestingly, *sox10* transcripts were also detected in CMs in a recently published single-cell transcriptome of zebrafish embryos (Wagner et al., 2018), further supporting our findings of a *sox10*$^+$ CM population in the zebrafish heart. Moreover, here, we also report *sox10* expression in *sox10*-derived CMs, supporting that our driver lines recapitulate expression of the endogenous gene. The biological pathways enriched in *sox10*-derived CMs compared to the rest of the ventricular myocardium were related to developmental processes, metabolism, and cell proliferation. This gene signature could be key for their increased contribution to the regenerated myocardium. The fact that *sox10*-derived cells upregulate more genes in response to injury than other ventricular CMs could suggest that they are epigenetically less repressed and therefore more sensitive to injury response and prone to contribute to heart regeneration.

An active *sox10* promoter might represent a particular state of CMs. Alternatively, CMs with an active *sox10* promoter might represent a distinct CM population in the zebrafish heart with high regenerative capacity. Understanding if cardiac *sox10*$^+$ cells are unique to this species or shared in mammals might help us understand the basis of regenerative capacity.

STAR★METHODS

Detailed methods are provided in the online version of this paper and include the following:

- KEY RESOURCES TABLE
- LEAD CONTACT AND MATERIALS AVAILABILITY
- EXPERIMENTAL MODEL AND SUBJECT DETAILS
- METHOD DETAILS
  - Generation of Tg(sox10:CreER^{T2})cn17
  - 4-Hydroxytamoxifen administration
  - Cryoinjury and analysis of the injured area
  - Metronidazole administration
  - BrdU administration
  - Histological staining
  - Cardiac imaging by echocardiography
  - Immunofluorescence on sections
  - Whole mount heart imaging and image processing
  - Imaging of larvae *in vivo*
  - RNAscope 2.5HD Detection Reagent (RED) - Immunofluorescence method
  - Disaggregation of zebrafish hearts, cardiomyocytes sorting and RNA-Seq library production
  - Bioinformatics analysis
- QUANTIFICATION AND STATISTICAL ANALYSIS
- DATA AND CODE AVAILABILITY

SUPPLEMENTAL INFORMATION

Supplemental Information can be found online at https://doi.org/10.1016/j.celrep.2019.09.041.

ACKNOWLEDGMENTS

We are grateful to Juan Manuel González-Rosa, Fernando Rodríguez-Pascual, Tilly Mommersteeg, Marianne Bronner, Joseph Yost, and Lukas Sommer for discussion and for sharing unpublished results; Lorena Flores and Ana Vanesa Alonso for help with echocardiography; Jonathan Landry for bioinformatics advice; Ricardo Costa for generating *Tg(sox10:CreER^{T2})cn17*; and Ronja Baal for fish husbandry. We thank the Animal facility, Histology, Cellomics, and Microscopy Units from CNIC; the MIC-Bern Unit and Cellomics Unit at the University of Bern; and Ken Poss, Robert Kelsh, and Alessandro Mongera for sharing fish lines. This work has been funded by the Spanish Ministry of Economy and Competitiveness (BFU2014–56970–P), the Swiss National Science Foundation (grant 31003A_159721), the ERC (starting grant 337703–zebra–Heart), Comunidad de Madrid (FIBROTEAM S2010/BMD-2321), and co-funding by Fondo Europeo de Desarrollo Regional (FEDER). I.J.M. was supported by Marie Curie Slodowska fellowship (PIEF-GA-2012-330728). D.F. was supported by BtRAIN (European Brain Barriers Training Network) (H2020-MSCA-ITN-2015, n°675619). The CNIC is supported by the Instituto de Salud Carlos III (ISCIII), the Ministerio de Ciencia, Innovación y Universidades (MCNU), and the Pro CNIC Foundation, and is a Severo Ochoa Center of Excellence (SEV-2015-0505).

AUTHOR CONTRIBUTIONS

M.S.-M. performed most of the experiments, prepared figures, and contributed to manuscript writing. I.J.M. performed experiments and supervised M.P.-L., who made the initial observation of a contribution of *sox10*-derived cells to regeneration. M.G.-C. and X.L. helped with experiments and were responsible for fish line maintenance. H.S.-I. generated the *vmBRN* line. G.G.-M. analyzed ultrasound data. D.P. and V.B. contributed to RNA-seq. M.-A.B., D.M.F.-F., and R.B. contributed to bioinformatics analysis. N.M. designed and interpreted the experiments, wrote the manuscript, and secured funding.

DECLARATION OF INTERESTS

The authors declare no competing interests.

Received: January 11, 2019
Revised: June 5, 2019
Accepted: September 13, 2019
Published: October 22, 2019

REFERENCES

Abdul-Wajid, S., Demarest, B.L., and Yost, H.J. (2018). Loss of embryonic neural crest derived cardiomyocytes causes adult onset hypertrophic cardiomyopathy in zebrafish. Nat. Commun. *9*, 4603.

Andrews, S. (2010). FastQC: a quality control tool for high throughput sequence data. http://www.bioinformatics.babraham.ac.uk/projects/fastqc.

Ashburner, M., Ball, C.A., Blake, J.A., Botstein, D., Butler, H., Cherry, J.M., Davis, A.P., Dolinski, K., Dwight, S.S., Eppig, J.T., et al.; The Gene Ontology Consortium (2000). Gene ontology: tool for the unification of biology. Nat. Genet. *25*, 25–29.

Auer, T.O., Duroure, K., De Cian, A., Concordet, J.P., and Del Bene, F. (2014). Highly efficient CRISPR/Cas9-mediated knock-in in zebrafish by homology-independent DNA repair. Genome Res. *24*, 142–153.

Carney, T.J., Dutton, K.A., Greenhill, E., Delfino-Machín, M., Dufourcq, P., Blader, P., and Kelsh, R.N. (2006). A direct role for Sox10 in specification of neural crest-derived sensory neurons. Development *133*, 4619–4630.

Cavanaugh, A.M., Huang, J., and Chen, J.N. (2015). Two developmentally distinct populations of neural crest cells contribute to the zebrafish heart. Dev. Biol. *404*, 103–112.

Curado, S., Stainier, D.Y., and Anderson, R.M. (2008). Nitroreductase-mediated cell/tissue ablation in zebrafish: a spatially and temporally controlled ablation method with applications in developmental and regeneration studies. Nat. Protoc. *3*, 948–954.

de Pater, E., Clijsters, L., Marques, S.R., Lin, Y.F., Garavito-Aguilar, Z.V., Yelon, D., and Bakkers, J. (2009). Distinct phases of cardiomyocyte differentiation regulate growth of the zebrafish heart. Development *136*, 1633–1641.

Durinck, S., Moreau, Y., Kasprzyk, A., Davis, S., De Moor, B., Brazma, A., and Huber, W. (2005). BioMart and Bioconductor: a powerful link between biological databases and microarray data analysis. Bioinformatics *21*, 3439–3440.

Felker, A., Nieuwenhuize, S., Dolbois, A., Blazkova, K., Hess, C., Low, L.W., Burger, S., Samson, N., Carney, T.J., Bartunek, P., et al. (2016). In Vivo Performance and Properties of Tamoxifen Metabolites for CreERT2 Control. PLoS ONE *11*, e0152989.

Garrity, D.M., Childs, S., and Fishman, M.C. (2002). The heartstrings mutation in zebrafish causes heart/fin Tbx5 deficiency syndrome. Development *129*, 4635–4645.

González-Rosa, J.M., and Mercader, N. (2012). Cryoinjury as a myocardial infarction model for the study of cardiac regeneration in the zebrafish. Nat. Protoc. *7*, 782–788.

González-Rosa, J.M., Martín, V., Peralta, M., Torres, M., and Mercader, N. (2011). Extensive scar formation and regression during heart regeneration after cryoinjury in zebrafish. Development *138*, 1663–1674.

González-Rosa, J.M., Guzmán-Martínez, G., Marques, I.J., Sánchez-Iranzo, H., Jiménez-Borreguero, L.J., and Mercader, N. (2014). Use of echocardiography reveals reestablishment of ventricular pumping efficiency and partial ventricular wall motion recovery upon ventricular cryoinjury in the zebrafish. PLoS ONE *9*, e115604.

González-Rosa, J.M., Burns, C.E., and Burns, C.G. (2017). Zebrafish heart regeneration: 15 years of discoveries. Regeneration (Oxf.) *4*, 105–123.

Grajevskaja, V., Camerota, D., Bellipanni, G., Balciuniene, J., and Balciunas, D. (2018). Analysis of a conditional gene trap reveals that tbx5a is required for heart regeneration in zebrafish. PLoS ONE *13*, e0197293.

Gupta, V., and Poss, K.D. (2012). Clonally dominant cardiomyocytes direct heart morphogenesis. Nature *484*, 479–484.

Gupta, V., Gemberling, M., Karra, R., Rosenfeld, G.E., Evans, T., and Poss, K.D. (2013). An injury-responsive gata4 program shapes the zebrafish cardiac ventricle. Curr. Biol. *23*, 1221–1227.

Iyengar, S., Kasheta, M., and Ceol, C.J. (2015). Poised regeneration of zebrafish melanocytes involves direct differentiation and concurrent replenishment of tissue-resident progenitor cells. Dev. Cell *33*, 631–643.

Jopling, C., Sleep, E., Raya, M., Martí, M., Raya, A., and Izpisúa Belmonte, J.C. (2010). Zebrafish heart regeneration occurs by cardiomyocyte dedifferentiation and proliferation. Nature *464*, 606–609.

Kanehisa, M., and Goto, S. (2000). KEGG: Kyoto Encyclopedia of Genes and Genomes. Nucleic Acids Res. *28*, 27–30.

Kikuchi, K. (2014). Advances in understanding the mechanism of zebrafish heart regeneration. Stem Cell Res. (Amst.) *13* (*3 Pt B, 3PB*), 542–555.

Kikuchi, K., Holdway, J.E., Werdich, A.A., Anderson, R.M., Fang, Y., Egnaczyk, G.F., Evans, T., Macrae, C.A., Stainier, D.Y., and Poss, K.D. (2010). Primary contribution to zebrafish heart regeneration by gata4(+) cardiomyocytes. Nature *464*, 601–605.

Kim, D., Langmead, B., and Salzberg, S.L. (2015). HISAT: a fast spliced aligner with low memory requirements. Nat. Methods *12*, 357–360.

Kuo, C.T., Morrisey, E.E., Anandappa, R., Sigrist, K., Lu, M.M., Parmacek, M.S., Soudais, C., and Leiden, J.M. (1997). GATA4 transcription factor is required for ventral morphogenesis and heart tube formation. Genes Dev. *11*, 1048–1060.

Lepilina, A., Coon, A.N., Kikuchi, K., Holdway, J.E., Roberts, R.W., Burns, C.G., and Poss, K.D. (2006). A dynamic epicardial injury response supports progenitor cell activity during zebrafish heart regeneration. Cell *127*, 607–619.

Lerman, D.A., Alotti, N., Ume, K.L., and Péault, B. (2016). Cardiac repair and regeneration: the value of cell therapies. Eur. Cardiol. *11*, 43–48.

Li, Y.X., Zdanowicz, M., Young, L., Kumiski, D., Leatherbury, L., and Kirby, M.L. (2003). Cardiac neural crest in zebrafish embryos contributes to myocardial cell lineage and early heart function. Dev. Dyn. *226*, 540–550.

Liao, Y., Smyth, G.K., and Shi, W. (2014). featureCounts: an efficient general purpose program for assigning sequence reads to genomic features. Bioinformatics *30*, 923–930.

Liberzon, A., Birger, C., Thorvaldsdóttir, H., Ghandi, M., Mesirov, J.P., and Tamayo, P. (2015). The Molecular Signatures Database (MSigDB) hallmark gene set collection. Cell Syst. *1*, 417–425.

Mahmoud, A.I., O'Meara, C.C., Gemberling, M., Zhao, L., Bryant, D.M., Zheng, R., Gannon, J.B., Cai, L., Choi, W.Y., Egnaczyk, G.F., et al. (2015). Nerves regulate cardiomyocyte proliferation and heart regeneration. Dev. Cell *34*, 387–399.

Molkentin, J.D., Lin, Q., Duncan, S.A., and Olson, E.N. (1997). Requirement of the transcription factor GATA4 for heart tube formation and ventral morphogenesis. Genes Dev. *11*, 1061–1072.

Mongera, A., Singh, A.P., Levesque, M.P., Chen, Y.Y., Konstantinidis, P., and Nüsslein-Volhard, C. (2013). Genetic lineage labeling in zebrafish uncovers novel neural crest contributions to the head, including gill pillar cells. Development *140*, 916–925.

Mosimann, C., Kaufman, C.K., Li, P., Pugach, E.K., Tamplin, O.J., and Zon, L.I. (2011). Ubiquitous transgene expression and Cre-based recombination driven by the ubiquitin promoter in zebrafish. Development *138*, 169–177.

Mosimann, C., Panáková, D., Werdich, A.A., Musso, G., Burger, A., Lawson, K.L., Carr, L.A., Nevis, K.R., Sabeh, M.K., Zhou, Y., et al. (2015). Chamber identity programs drive early functional partitioning of the heart. Nat. Commun. *6*, 8146.

Pfefferli, C., and Jaźwińska, A. (2017). The careg element reveals a common regulation of regeneration in the zebrafish myocardium and fin. Nat. Commun. *8*, 15151.

Picelli, S., Faridani, O.R., Björklund, A.K., Winberg, G., Sagasser, S., and Sandberg, R. (2014). Full-length RNA-seq from single cells using Smart-seq2. Nat. Protoc. *9*, 171–181.

Prabhu, S.D., and Frangogiannis, N.G. (2016). The biological basis for cardiac repair after myocardial infarction: from inflammation to fibrosis. Circ. Res. *119*, 91–112.

R Core Team (2018). R: A language and environment for statistical computing (R Foundation for Statistical Computing). https://www.R-project.org/.

Sánchez-Iranzo, H., Galardi-Castilla, M., Minguillón, C., Sanz-Morejón, A., González-Rosa, J.M., Felker, A., Ernst, A., Guzmán-Martínez, G., Mosimann, C., and Mercader, N. (2018). Tbx5a lineage tracing shows cardiomyocyte plasticity during zebrafish heart regeneration. Nat. Commun. *9*, 428.

Sato, M., and Yost, H.J. (2003). Cardiac neural crest contributes to cardiomyogenesis in zebrafish. Dev. Biol. *257*, 127–139.

Schindler, Y.L., Garske, K.M., Wang, J., Firulli, B.A., Firulli, A.B., Poss, K.D., and Yelon, D. (2014). Hand2 elevates cardiomyocyte production during zebrafish heart development and regeneration. Development *141*, 3112–3122.

Sereti, K.I., Nguyen, N.B., Kamran, P., Zhao, P., Ranjbarvaziri, S., Park, S., Sabri, S., Engel, J.L., Sung, K., Kulkarni, R.P., et al. (2018). Analysis of cardiomyocyte clonal expansion during mouse heart development and injury. Nat. Commun. *9*, 754.

Sergushichev, A. (2016). An algorithm for fast preranked gene set enrichment analysis using cumulative statistic calculation. bioRxiv. https://doi.org/10.1101/060012.

Srivastava, D., Thomas, T., Lin, Q., Kirby, M.L., Brown, D., and Olson, E.N. (1997). Regulation of cardiac mesodermal and neural crest development by the bHLH transcription factor, dHAND. Nat. Genet. *16*, 154–160.

Susaki, E.A., Tainaka, K., Perrin, D., Yukinaga, H., Kuno, A., and Ueda, H.R. (2015). Advanced CUBIC protocols for whole-brain and whole-body clearing and imaging. Nat. Protoc. *10*, 1709–1727.

Tamura, Y., Sano, M., Nakamura, H., Ito, K., Sato, Y., Shinmura, K., Ieda, M., Fujita, J., Kurosawa, H., Ogawa, S., et al. (2016). Neural crest-derived resident cardiac cells contribute to the restoration of adrenergic function of transplanted heart in rodent. Cardiovasc. Res. *109*, 350–357.

Tessadori, F., van Weerd, J.H., Burkhard, S.B., Verkerk, A.O., de Pater, E., Boukens, B.J., Vink, A., Christoffels, V.M., and Bakkers, J. (2012). Identification and functional characterization of cardiac pacemaker cells in zebrafish. PLoS ONE *7*, e47644.

Wagner, D.E., Weinreb, C., Collins, Z.M., Briggs, J.A., Megason, S.G., and Klein, A.M. (2018). Single-cell mapping of gene expression landscapes and lineage in the zebrafish embryo. Science *360*, 981–987.

Wang, J., Panáková, D., Kikuchi, K., Holdway, J.E., Gemberling, M., Burris, J.S., Singh, S.P., Dickson, A.L., Lin, Y.F., Sabeh, M.K., et al. (2011). The regenerative capacity of zebrafish reverses cardiac failure caused by genetic cardiomyocyte depletion. Development *138*, 3421–3430.

Wang, L., Wang, S., and Li, W. (2012). RSeQC: quality control of RNA-seq experiments. Bioinformatics *28*, 2184–2185.

White, R.M., Sessa, A., Burke, C., Bowman, T., LeBlanc, J., Ceol, C., Bourque, C., Dovey, M., Goessling, W., Burns, C.E., and Zon, L.I. (2008). Transparent adult zebrafish as a tool for in vivo transplantation analysis. Cell Stem Cell *2*, 183–189.

White, I.A., Gordon, J., Balkan, W., and Hare, J.M. (2015). Sympathetic reinnervation is required for mammalian cardiac regeneration. Circ. Res. *117*, 990–994.

Wills, A.A., Holdway, J.E., Major, R.J., and Poss, K.D. (2008). Regulated addition of new myocardial and epicardial cells fosters homeostatic cardiac growth and maintenance in adult zebrafish. Development *135*, 183–192.

Xiang, F.L., Guo, M., and Yutzey, K.E. (2016). Overexpression of Tbx20 in adult cardiomyocytes promotes proliferation and improves cardiac function after myocardial infarction. Circulation *133*, 1081–1092.

Yu, G., Wang, L.G., Han, Y., and He, Q.Y. (2012). clusterProfiler: an R package for comparing biological themes among gene clusters. OMICS *16*, 284–287.

Zhou, Y., Cashman, T.J., Nevis, K.R., Obregon, P., Carney, S.A., Liu, Y., Gu, A., Mosimann, C., Sondalle, S., Peterson, R.E., et al. (2011). Latent TGF-β binding protein 3 identifies a second heart field in zebrafish. Nature *474*, 645–648.

STAR★METHODS

KEY RESOURCES TABLE

REAGENT or RESOURCE	SOURCE	IDENTIFIER
Antibodies		
Mouse monoclonal anti MF20	DSHB	Cat# MF 20, RRID:AB_2147781
Mouse monoclonal anti tropomyosin	DSHB	Cat# CH1, RRID:AB_2205770
Mouse monoclonal anti BrdU	BD PharMingen	Cat# 347583, RRID:AB_400327
Rat monoclonal anti mCherry	Thermo Fisher Scientific	Cat# M11217, RRID:AB_2536611
Rabbit polyclonal anti-Tyrosine Hydroxylase	Sigma Aldrich	Cat# T8700, RRID:AB_1080430
Rabbit polyclonal anti-RFP	Abcam	Cat# ab34771, RRID:AB_777699
Biotin-SP-conjugated AffiniPure anti-rabbit IgG (H+L)	Jackson Immuno Research Laboratories	Cat# 713-065-003, RRID:AB_2340715
Goat anti-Rabbit IgG (H+L) Secondary Antibody, Alexa Fluor® 568 conjugate	Thermo Fisher Scientific	Cat# S-11226, RRID:AB_2315774
Goat anti-Mouse IgG1 Secondary Antibody, Alexa Fluor® 488 conjugate	Thermo Fisher Scientific	Cat# A-21121; RRID:AB_2535764
Goat anti-Mouse IgG1 Secondary Antibody, Alexa Fluor® 568 conjugate	Thermo Fisher Scientific	Cat# A-21124; RRID:AB_2535766
Goat anti-Mouse IgG1 Secondary Antibody, Alexa Fluor® 647 conjugate	Thermo Fisher Scientific	Cat# A-21240; RRID:AB_2535809
Goat anti-Mouse IgG2b Secondary Antibody, Alexa Fluor® 488 conjugate	Thermo Fisher Scientific	Cat# A-21242, RRID:AB_253581
Chemicals, Peptides, and Recombinant Proteins		
4',6-Diamidino-2-phenylindole dihydrochloride (DAPI)	Thermo Fisher Scientific	Cat# D3571
5-bromo-2′-deoxyuridine (BrdU)	Sigma Aldrich	Cat# 59-14-3
4-hydroxytamoxifen	Sigma Aldrich	Cat#T5648
2,3-butanedione monoxime	Sigma-Aldrich	Cat#B0753
Metronidazole	Sigma-Aldrich	Cat#M3761
Software and Algorithms		
Fiji	NIH	SCR_002285
GraphPad Prism 7	GraphPad Software	SCR_002798
Imaris software 8.2	Bitplane	SCR_007370
Ingenuity Pathway Analysis	QIAGEN	SCR_008653
DESeq2 v1.20.00	SciCrunch	SCR_015687
R Project for Statistical Computing	SciCrunch	SCR_001905
Gene Ontology	SciCrunch	SCR_002811
KEGG	SciCrunch	SCR_012773
clusterProfiler	SciCrunch	SCR_016884
MSigDB	SciCrunch	SCR_016863
biomaRt	SciCrunch	SCR_002987
Experimental Models: Organisms/Strains		
Zebrafish: Tg(*−4.9sox10:egfp*)^{ba2}	(Carney et al., 2006)	ZDB-ALT-050913-4
Zebrafish: Tg(*sox10:CreER*^{T2}*,myl7:GFP*)^{t007}	(Mongera et al., 2013)	ZDB-ALT-130322-3
Zebrafish: Tg(*-3.5ubi:loxP-EGFP-loxP-mCherry*)^{cz1701}	(Mosimann et al., 2011)	ZDB-TGCONSTRCT-110124-1
Zebrafish: Tg(*actb2:loxP-mCherry-loxP-DipTox*)^{pd36}	(Wang et al., 2011)	ZDB-ALT-110914-1
Zebrafish: Tg(*vmhcl:loxP-myctagBFP-STOP-loxP-NTR-mCherry*)^{cn5}	(Sánchez-Iranzo et al., 2018)	ZDB-ALT-170711-2
Zebrafish: Tg(*sox10:CreER*^{T2})cn17	This manuscript	n/a

LEAD CONTACT AND MATERIALS AVAILABILITY

Further information and requests for resources and reagents should be directed to and will be fulfilled by the Lead Contact, Nadia Mercader (nadia.mercader@ana.unibe.ch).

All unique/stable reagents generated in this study are available from the Lead Contact with a completed Materials Transfer Agreement.

EXPERIMENTAL MODEL AND SUBJECT DETAILS

Experiments were conducted with zebrafish embryos, juveniles and adults aged 6–18 months, raised at maximal 5 fish/l and maintained under the same environmental conditions: 27.5-28°C, 650-700μs/cm, pH 7.5, the lighting conditions were 14:10 hours (light: dark) and 10% of water exchange a day. Experiments were approved by the Community of Madrid "Dirección General de Medio Ambiente" in Spain, the Landesamt für Verbraucherschutz Thüringen, Germany and the "Amt für Landwirtschaft und Natur" from the Canton of Bern, Switzerland. All animal procedures conformed to EU Directive 86/609/EEC and Recommendation 2007/526/EC regarding the protection of animals used for experimental and other scientific purposes, enforced in Spanish law under Real Decreto 1201/2005. Experiments in Switzerland were conducted under the licenses BE95/15 and BE64/18. For longitudinal experiments, the selected animals were grown together with Casper (White et al., 2008) zebrafish until heart collection at the density as explained above.

METHOD DETAILS

Generation of Tg(sox10:CreER^{T2})cn17

In order to remove the reporter *myl7:GFP* from the line Tg(*sox10:CreER^{T2},myl7:GFP*)^{t007} (Mongera et al., 2013) we injected the guide RNA sgRNA *eGFP*1 GGCGAGGGCGATGCCACCTA targeting *GFP* (Auer et al., 2014) together with Cas9 protein into 1-cell stage embryos and raised offspring without GFP expression in the heart. Germline transmission was evaluated by crossing F0 into *ubi:Switch* and inducing recombination with 4-OHT administration. This line was used for the experiments shown in Figures 5, 6, and 7.

4-Hydroxytamoxifen administration

4-hydroxytamoxifen (4-OHT; Sigma H7904) was administered at the indicated times and treatments were performed overnight. Prior to administration, the 10 mM stock (dissolved in 99.8% ethanol) was heated for 10 minutes at 65°C (Felker et al., 2016). For genetic labeling in *Tg(sox10:CreER^{T2}; ubb:Switch)* embryos, 4-OHT was administered at 5-10 μM from 12 to 48 hours post-fertilization (hpf). For lineage tracing studies in adult fish, 4-OHT was administered at 10 μM overnight.

Cryoinjury and analysis of the injured area

Cryoinjury was performed as previously described (González-Rosa and Mercader, 2012). Adult fish were anesthetized with 0.032% tricaine (Sigma, St Louis, MO, USA) and their pericardial cavity opened with microdissection scissors to expose the heart. A copper filament cooled in liquid nitrogen was placed on the ventricular surface of the heart until thawing. After surgery, animals were revived by gently directing water to their gills using a plastic Pasteur pipette.

For analysis of regeneration, animals were euthanized at different times post-injury by immersion in 0.16% Tricaine (Sigma, St Louis, MO, USA), and hearts were dissected in media containing 2 U/ml heparin and 0.1 M KCl. For quantification of injured area on paraffin sections as shown in Figures 1F and 1G, color deconvolution tool and color threshold tool (ImageJ Software) were used to segment and measure the injured and uninjured myocardium in μm^2.

Metronidazole administration

For genetic ablation using Metronidazole (Mtz; Sigma, M3761), Mtz was diluted in fish water at 10 mM with DMSO at 0.2% and administered overnight.

BrdU administration

Animals were injected intraperitoneally either at 6 dpi or at 7 dpi and 29 dpi with 30 μl of 2.5 mg/ml of 5-Bromo-2-deoxyuridine (BrdU, B5002-1G, Sigma). Hearts were collected and processed for analysis at 7 dpi and 30 dpi. To calculate the proliferation index, cryosections were immunostained with anti-BrdU, anti-RFP, and anti-MHC antibodies as described below. At least 3 ventricular sections were imaged for each heart. MHC$^+$/mCherry$^+$/BrdU$^+$ CMs compared to MHC$^+$/mCherry$^-$/BrdU$^+$ CMs were counted manually using ImageJ software.

Histological staining

Hearts were fixed in 2 or 4% paraformaldehyde (PFA) in phosphate-buffered saline (PBS) overnight at 4°C. Samples were then washed in PBS, dehydrated through graded alcohols, washed in Xylol and embedded in paraffin wax. All histological staining were performed on 7 μm paraffin sections cut on a microtome (Leica and Reichert-Jung), mounted on Superfrost slides (Fisher Scientific), and dried overnight at 37°C. Sections were deparaffinized in xylol, rehydrated and washed in distilled water. Connective tissue was stained using Acid Fuchsine Orange G (AFOG) (González-Rosa et al., 2014). ImageJ software was used to quantify cryoinjured area in uninjured and injured hearts.

Cardiac imaging by echocardiography

Animals were anaesthetized by immersion for approx. 5 min in a combined solution of 60 mM Tricaine/3 mM Isoflurane dissolved in fish tank water (González-Rosa et al., 2014). Individual fish were placed ventral side up on a custom-made sponge in a Petri dish filled with the anesthetic solution. Two-dimensional (2D) high-resolution real-time *in vivo* images were obtained with the Vevo2100 Imaging System through a RMV708 (22-83 MHz) scanhead (VisualSonics, Toronto, Canada). Imaging and image analysis were performed as described (González-Rosa et al., 2014).

Immunofluorescence on sections

Heart sections were deparaffinized, rehydrated and washed in distilled water. Epitope recovery was carried out by boiling in citrate buffer (pH 6.0) for 20 min in a microwave at full power. Sections were permeabilized with Triton X-100 0.5% for 15 min. Non-specific binding sites were saturated by incubation for 1 hour in blocking solution (5% BSA, 5% goat serum, 0.1% Tween-20). Endogenous biotin was blocked with the avidin-biotin blocking kit (Vector, Burlingame, CA, USA). For tyramides amplification, slides were blocked in 3% H_20_2-PBS for 20 minutes. Slides were incubated overnight with the following primary antibodies at 4°C: anti-myosin heavy chain (MF20, DSHB; diluted 1:20), anti-tropomyosin (CH1, DSHB; diluted 1:20), anti-RFP (Abcam, diluted 1:150), anti-BrdU (BD PharMingen diluted 1:100), anti-mCherry (16D47, Thermo Fisher Scientific, diluted 1:150), anti-Tyrosine Hydroxylase (Sigma, diluted 1:150), biotinylated anti-rabbit (Thermo Fisher Scientific, 1:150), HRP (DAKO, 1:250). Antibody signals were detected with streptavidin- or Alexa (488, 568, 633)-conjugated secondary antibodies (Invitrogen; each diluted 1:250) and streptavidin-Cy3 (Molecular Probes, SA1010) after incubation for 1 hour at room temperature. For tyramides amplification (Merck, TSA Plus Cyanine 3 System, Cat# NEL744001KT), Cy3 was conjugated for 4 minutes. Nuclei were stained with 4',6-Diamidino-2-phenylindole dihydrochloride (DAPI) (1:1000, Merck) and slides were mounted in DAKO fluorescent mounting medium (DAKO). Images were analyzed and processed using ImageJ.

Cryosections were prepared as above with the following modifications: heart sections were incubated for 30 min in PBS at 37°C to remove the gelatin. They were washed two more times with PBS at room temperature and then immunofluorescence proceeded as for paraffin sections.

Whole mount heart imaging and image processing

Hearts were incubated with block solution (5% BSA, 5% got serum, 0.1% Tween-20) for two days and incubated in primary antibody for three days at 4°C in rocking agitation. We washed hearts three times with PBS Tw 0.1% for 1 hour. Secondary and tertiary antibody incubations were performed for two days at 4°C in rocking agitation. Again, we washed hearts three times with PBS Tw 0.1% for 1 hour. Then, hearts were fixed in 2% PFA overnight. We used CUBIC reagent (Susaki et al., 2015) for tissue clearing. Hearts were incubated in CUBIC reagent 1 for three days at 37°C, washed in 0.1% PBS/Tween 20 three times for 20 minutes, whole mount immunofluorescence was performed and samples were incubated afterward in CUBIC reagent 2 for three further days at room temperature. Hearts were mounted on a glass bottom culture dish (MatTek Corporation) for confocal acquisition. Whole heart images were obtained with Zeiss LSM 780, Zeiss LSM 880, and Leica TCS SP8 confocal microscopes with a 10 dry, 20 × dry and 40x water-dipping lenses. Images were recorded at 512 × 512, 1024 × 1024 and 2048x 2048 resolution. Tile scan and z stack of each heart was acquired. The proportion of $mCherry^+/MHC^+$ versus all MHC^+ CMs was evaluated with Imaris software 8.2 (BITPLANE). A distance transformation algorithm (Imaris software 8.2) was used to study the distance of $mCherry^+/MHC^+$ CMs to the injured or apex area. Adult zebrafish heart representing embryonic *sox10*-derived CMs in the Figures S2E and S2F .lsm raw data file was converted to .ims (Imaris file extension) by Imaris software 8.2 (BITPLANE). The Imaris image was saved as TIFF, with a larger field of view than the original file. This corresponds to the images shown in the panels.

Imaging of larvae *in vivo*

Double transgenic larvae *Tg*(*sox10:CreER*^{T2};*ubb:Switch*) were transferred to E3 medium containing 0.2 mg/ml tricaine and 0.0033% PTU and immobilized using 0.7% agarose (Bio-Rad Low Melting agarose, #Cat 161-3111) in a glass bottom microwell-dish (MatTek Corporation). Zebrafish hearts were scanned using bidirectionally acquisition with SP5 confocal microscope (Leica SP5) using a 20x glycerol lens. Larvae were carefully removed from the agarose embedding and were grown to adults in fish tanks together with Casper fish. Adult zebrafish hearts were collected, fixed in 2% PFA overnight and scanned with LSM 700 Confocal microscope using 20x dry lens (Zeiss). 3D reconstruction and analysis were done using Imaris Software 8.2.

RNAscope 2.5HD Detection Reagent (RED) - Immunofluorescence method

All the hearts were fixed at room temperature (RT) for 24h in 10% Neutral Formalin Buffer (NFB). After fixation, samples were washed 3 times for 10 minutes in 1x PBS. Dehydration process was performed using a standard ethanol series (10 minutes each), followed by two xylol washes (5 minutes each) and embedding of tissues was carry out.

Paraffin blocks were cut with microtome (Microm) at 6μm thickness per section, collected in the water bath with SuperFrost slides and baked slides in a dry oven for one hour at 60°C. After that, slides were dewaxed by incubating 2 times for 5 minutes in xylol, 2 times for 2 minutes in 100% ethanol and dried in a dry oven for 5 minutes at 60°C. They were then, permeabilized with hydrogen peroxide (ACD#322381) for 10 minutes at RT and washed 2 times for 1 minute in distilled water.

Target retrieval (ACD, #322000) was performed for 15 minutes at 100°C. Slides were then washed for 15 s in distilled water and 100% ethanol for 3 minutes and dried for 5 minutes at 60°C. Afterward PAP Pen (Vector, #H-4000) was used to create a hydrophobic barrier for each section. After that, slides were incubated with protease Plus (ACD#322381) for 5 minutes at 40°C and washed in distilled water twice.

Two probes were designed for the experiment (Dr-Sox10 and negative control probe-DapB). Hybridization was done by incubating the sections with the the probes for 2 hours at 40°C, followed by 2 washes of 2 minutes in washing buffer (ACD, #310091).

Finally, signal detection was done by using the RNAscope 2.5 HD Detection Reagent-RED (ACD, #322360) as follows: incubation with AMP1 for 30min at 40°C; washing with wash buffer AMP2 for 15min at 40°C, wash buffer AMP3 for 30min at 40°C, wash buffer AMP4 for 15min at 40°C, wash buffer AMP5 for 30min at 40°C, wash buffer AMP6 for 15min at 40°C, wash buffer RED working solution for 10min at RT, and wash in distilled water twice for 5 minutes.

Disaggregation of zebrafish hearts, cardiomyocytes sorting and RNA-Seq library production

Uninjured and injured recombined adult zebrafish *sox10:CreER^{T2};vmhcl:loxP-tagBFP-loxP-mCherry-NTR* hearts were collected 12 days after the final 4-OHT pulse or 7 dpi respectively, and processed according to previous protocols (Sánchez-Iranzo et al., 2018; Tessadori et al., 2012). Atrium and *bulbus arteriosus* were removed to obtain only the ventricle. A total of 15 uninjured and 18 injured hearts were used to create 5 pools (comprised of 3 hearts each) of uninjured hearts and 6 pools (each again comprised of 3 hearts) for injured hearts. From each pool 20 CMs were FAC-sorted.

mCherry^{+}, mCherry;BFP^{+} and BFP^{-} CMs were sorted in 0.2 mL tubes in lysis buffer using Synergy 4L Cell Sorter and immediately frozen at −80°C. Smart-Seq2 RNA library preparation was performed according to previous protocols (Picelli et al., 2014). An Agilent Bioanalyzer was used to measure quality of library preparation. Library concentration was measured using the Qubit fluorometer (ThermoFisher Scientific). Final libraries concentration was 10 nM. Libraries were sequenced using Illumina NextSeq 500.

Bioinformatics analysis

BCL files were converted to FastQ files, using bcl2fastq2 (v2.20.0.422 – Illumina). Reads were mapped to the reference genome (Ensembl build 11, release 94) using Hisat2, version 2.1.0 (Kim et al., 2015) and counting was performed using featureCounts, version 1.6.0 (Liao et al., 2014). Multiple quality control features were measured and observed using both FastQC, version 0.11.5 (Andrews, 2010) and RseQC, version 2.6.4 (Wang et al., 2012). From 44 sequenced samples 18 were discarded as they did not pass the quality control. For bioinformatics analysis, we compared mCherry^{+} (mCherry^{+}, mCherry^{+}BFP^{+}) with mCherry^{-} (BFP^{+}) pools. The comparison was performed for samples extracted from uninjured and 7 dpi hearts. Downstream analysis was performed in R, version 3.5.1 (R Core Team, 2018).

Counts were normalized and differential expression between design groups was tested using package DESeq2 v.1.20.00 with no log2 fold change shrinkage (default betaPrior option for the latest versions of the tool). Principal component analysis (PCA) plots, volcano plots and heatmaps were generated using the ggplot2 package, version 3.0.0 (H. Wickham. ggplot2: Elegant Graphics for Data Analysis. Springer-Verlag New York, 2016.).

Further analyses were performed with DESeq2 results. For the enrichment we selected all the Gene Stable IDs and translated to *Mus musculus* Gene Stable IDs and obtained the ENTREZIDs and SYMBOLs using biomaRt package (Durinck et al., 2005). With the genes translated, the top differentially expressed genes (DEG) that passed FDR < 0.05 for Gene Ontology (GO) (Ashburner et al., 2000) over representation analysis (ORA) using clusterProfiler package (Yu et al., 2012).

Afterwards, we performed deeper analysis for overall gene expression with gene set enrichment analysis (GSEA). The differential gene expression results from DESeq2 were sorted by Log2FoldChange value. Kyoto Encyclopedia of Genes and Genomes (KEGG) (Kanehisa and Goto, 2000) and Molecular Signature Database (MsigDB) (Liberzon et al., 2015) using the Hallmarks collection were used for biological insight. For the GSEA analyses clusterProfiler and FGSEA packages (Sergushichev, 2016) were used with KEGG and MsigDB Hallmarks gene set respectively. For data representation only those with adjusted p value < 0.05 were considered significant of the results obtained.

Ingenuity pathway analysis core analysis (IPA, QIAGEN Inc., https://www.qiagenbioinformatics.com/products/ingenuity-pathway-analysis) was used to identify canonical pathways, functions and diseases related to our differentially expressed genes in uninjured and injured conditions.

QUANTIFICATION AND STATISTICAL ANALYSIS

Statistical analysis was performed using GraphPad. Shown are means and error bars represent SD in all graphs. The specific test used, exact value of n, explanation of what n represents, definition of center, dispersion and precision measures are indicated in each figure legend or citation in the main text. Normal distribution was tested to decide if a parametric or non-parametric test needed to be applied.

DATA AND CODE AVAILABILITY

RNA-seq data were deposited at Gene OmnibusDatabase: Gene Omnibus Database with reference GSE 133571. Raw data of images as well as statistical analysis has been uploaded at Mendeley Database: https://doi.org/10.17632/5h7z68ck98.2